Continental Shelf Research 282 (2024) 105323

Contents lists available at ScienceDirect

Continental Shelf Research

journal homepage: www.elsevier.com/locate/csr

Environmental factors affecting the distribution of deep-water rose shrimp (*Parapenaeus longirostris, Lucas, 1846*) abundance in the Strait of Sicily (Mediterranean Sea)

Francesco Bignami [a,*], Fabio Fiorentino [b,g], Germana Garofalo [b,i], Enrico Zambianchi [a,c], Simone Colella [a], Roberto Sorgente [d], Antonio Olita [e], Angela Landolfi [a], Federico Quattrocchi [h,i], Peter I. Miller [f]

[a] CNR-ISMAR SS Roma, via Fosso del Cavaliere 100, 00133, Rome, Italy
[b] CNR-IRBIM SS Mazara del Vallo, Via L. Vaccara 61, 91026, Mazara del Vallo, (TP), Italy
[c] Università degli Studi di Napoli "Parthenope" and CoNISMa, Naples, Italy
[d] CNR-IAS SS Oristano, Loc. Sa Mardini snc, 09170, Torregrande, Oristano, (OR), Italy
[e] CNR-ISAC Cagliari, c/o Dip. Fisica, Università di Cagliari Strada Pro.le Monserrato, Sestu Km. 0, 700 09042, Cagliari, (CA), Italy
[f] Remote Sensing Group, Plymouth Marine Laboratory, Prospect Place, Plymouth, PL1 3DH, UK
[g] SZN - Stazione Zoologica Anton Dohrn (SZN), Lungomare Cristoforo Colombo 4521, 90149, Palermo, Italy
[h] Department of Earth and Marine Sciences (DiSTeM), University of Palermo, I-90123, Palermo, Italy
[i] NBFC, National Biodiversity Future Center, Palermo, Italy

ARTICLE INFO

Keywords:
Deep-water rose shrimp
SST
Chlorophyll
Fronts
POC
Generalized additive models

ABSTRACT

The distribution of deep-water rose shrimp (*Parapenaeus longirostris*, FAO 3 alpha code DPS), the main target species of demersal fisheries in the Strait of Sicily, is investigated in relation to surface parameters and biogeochemical processes. Such processes are known to influence sea bottom habitats and may be particularly relevant to the Strait of Sicily because of its relative shallowness and high surface primary production. Shrimp abundances recorded during multi-annual and seasonal trawl surveys (2004–2008) are analyzed. A GAMM and GAM model analysis is performed comparing juvenile abundances to monthly mean spatial patterns of remotely-sensed sea surface temperature (SST) and surface chlorophyll (*chl*), as well as their frontal structures, with a time-lag of one month, given the pelagic behavior of DPS early life stages preceding settlement. Juvenile and total shrimp abundances are also compared to the flux of particulate organic carbon (POC) to the seabed. The POC flux is computed via 1-D and 3-D models simulating sinking, re-mineralization and horizontal advection and diffusion of surface POC. The latter is derived from surface primary production maps obtained from ocean color data. Results show that the abundance of the juvenile fraction of DPS is significantly correlated with depth, distance to SST fronts and the intensity of *chl* fronts (correlation R^2 = 80%). Furthermore, results strongly suggest the significant role of bottom POC flux in conditioning the distribution of DPS abundance, indicating that ecological processes occurring in surface waters influence food availability near the seabed in the investigated area.

1. Introduction

The deep-water rose shrimp (*Parapenaeus longirostris*; Lucas, 1846; hereafter DPS, after its FAO 3 alpha code) is a large-size decapod crustacean widely distributed in the Mediterranean Sea and the Atlantic Ocean, from the north of Spain to the southern waters of Angola (Sobrino et al., 2005). It is an epi-benthic species with a pelagic larval stage (Sobrino et al., 2005), showing a size-related bathymetric distribution, linked to the ontogenetic migration of juveniles from the continental shelf (50–200 m) to the upper slope, i.e. down to 500 m (Ardizzone et al., 1990; Politou et al., 2008). Reproduction occurs year-round (Levi et al., 1995; Mori et al., 2000b), thus the species shows

* Corresponding author. ISMAR-CNR Sede Secondaria di Roma, Via Fosso del Cavaliere 100, 00133, Roma, Italy.
E-mail addresses: francesco.bignami@artov.ismar.cnr.it (F. Bignami), fabio.fiorentino@irbim.cnr.it (F. Fiorentino), germana.garofalo@cnr.it (G. Garofalo), enrico.zambianchi@uniparthenope.it (E. Zambianchi), simone.colella@cnr.it (S. Colella), roberto.sorgente@cnr.it (R. Sorgente), antonio.olita@cnr.it (A. Olita), angela.landolfi@artov.ismar.cnr.it (A. Landolfi), quattrocchifederico@gmail.com (F. Quattrocchi), pim@pml.ac.uk (P.I. Miller).

https://doi.org/10.1016/j.csr.2024.105323
Received 20 February 2024; Received in revised form 20 June 2024; Accepted 31 August 2024
Available online 7 September 2024

a continuous recruitment pattern. Despite being prevalently benthic, DPS display also a pelagic behavior consisting of mostly nocturnal vertical migration for feeding, similarly to other shrimp species (Marin, 2009; Rodríguez-Climent et al., 2016). This is the most important crustacean species landed by Mediterranean trawl fisheries, amounting up to about 12,000 tons per year, or 23% of total crustacean landings in 2000–2008 (Knittweis et al., 2013). In terms of total yield, the most productive fleet targeting DPS is that operating in the Strait of Sicily (hereafter SoS), yielding about 60–70% of the total catch in the Mediterranean Sea (Knittweis et al., 2013).

The SoS is well known as one of the areas of the Mediterranean characterized by the occurrence of the Bakun (1998) triad processes of enrichment, concentration and retention of oceanic scalar properties (e.g. phytoplankton) by means of physical processes, both at regional and at smaller local scale along the south coast of Sicily (Agostini and Bakun, 2002; Patti et al., 2020). These processes occur due to semi-permanent oceanographic features including upwelling, frontal formations and mesoscale eddies (Piccioni et al., 1988; Béranger et al., 2004) and provide enhanced primary production and favor reproductive and recruitment habitats for many marine populations (Agostini and Bakun, 2002; Garcìa Lafuente, 2002).

Indeed, the influence of sea surface temperature (SST) and surface chlorophyll (*chl*) frontal structures on the abundance fluctuations and distribution of marine populations is well documented (e.g. Houghton and Marra, 1983; Demarcq and Faure, 2000; Klein and Lapeyre, 2009; Druon et al., 2011, 2021; Scales et al., 2014; Lévy et al., 2012; Zervoudaki et al., 2006). Also, in the SoS, strong correlations between relevant oceanographic features and the distribution of critical life stages of fishery resources have been observed not only for pelagic species (Garcìa Lafuente, 2002; Basilone et al., 2013; Falcini et al., 2015; Patti et al., 2020) but also for demersal ones (Abella et al., 2008; Druon et al., 2015; Gargano et al., 2017, 2022; Quattrocchi et al., 2019). The relative shallowness of the SoS, mostly <1000 m with large banks <200 m, and the high primary production observed in the upwelling-influenced zone closer to the Sicilian coasts (Piccioni et al., 1988; Buongiorno Nardelli et al., 1999; Askari, 1998, 2001; Bakun and Agostini, 2001; Bignami et al., 2008) suggest that the influence of surface processes on bottom ecology could be stronger there than in other deeper areas of the ocean.

As regards DPS reproduction, Fortibuoni et al. (2010) found that stable nurseries in the SoS were located on the outer Sicilian shelf, while persistent spawning areas occurred mostly between the outer shelf and the upper slope. Further, the study found that the geographic positions of both these stable critical areas were coherent with those of the semi-permanent mesoscale features (i.e. eddies) of the Strait of Sicily promoting biological retention, concentration and biogeochemical enrichment processes. Although no deterministic relationships between spatial/temporal dynamics of DPS abundance and ecological factors were investigated, the authors hypothesized that retention mechanisms allow the larvae and juveniles to stay in an area of enhanced primary and secondary production. Since DPS juveniles feed on micro- and mesoplankton prey (radiolarians, tintinnids, copepods and pteropods), these habitats should be particularly favorable for their feeding and growth (Nouar et al., 2011). On the other hand, larger DPS feed on small fishes, cephalopods and above all crustaceans (amphipods, copepods and ostracods) as well as sedentary preys in seabed sediments, mainly foraminifera and radiolarians but also polychaeta, bivalves and gastropods (Carlucci and Gancitano, 2015). DPS feeds also on organic detritus, the contribution of which seems to increase gradually with depth (Sobrino et al., 2005; Nouar et al., 2011). Therefore, also spawners could benefit from high food abundance occurring close to frontal systems and arriving at the seafloor, for gonad development (Fortibuoni et al., 2010).

The importance of the transport of phytodetritus from the surface layers to the bottom has also been highlighted by Cartes et al. (2018) for different life-stages of the deep-water shrimp *Aristeus antennatus* (Risso, 1816) across its full depth range (500–2200 m) in the western Mediterranean. In particular, spawning females were found in areas with lower near-bottom oxygen levels coupled with senescent marine snow. Conversely, mature males were found in grounds with higher oxygen levels, suggesting a dietary preference for mobile zooplanktonic preys that require more oxygen-rich environments. Finally, recruits preferred habitats with high near-bottom oxygen levels, low turbidity and sediments rich in organic matter, which are associated with high abundance of suprabenthic and benthic preys.

The tight coupling between the benthic and pelagic realms, driven by physical and biological processes, is crucial for nutrient cycling and energy flow in aquatic ecosystems (Polunin et al., 2001; Baustian et al., 2014). For instance, it is known that the fraction of particulate organic carbon (POC) formed by primary production in the euphotic layer and sinking at depth is an important source of carbon and energy for the demersal heterotrophic communities (Siegel and Deuser, 1997; Griffiths et al., 2017). Indeed, POC plays a key role in foraging the benthic community in highly productive waters (Biggs et al., 2008; Morse and Beazley, 2008; Muller-Karger et al., 2005). This is true, even though the vertical POC flux attenuates rapidly with depth, due to both abiotic (circulation dynamics) and biotic (bacterial respiration and zooplankton reworking) controls, the latter commonly described by a power-law function (Martin et al., 1987; Pace et al., 1987). Since no major rivers flow into the SoS, the riverine supply of nutrients and terrigenous organic material (plant debris, humic substances; Emerson and Hedges, 1988) can be considered negligible. Therefore, we hypothesize that the energy injections due to the POC flux originated from surface primary production at sea may have a major role in the distribution of DPS abundance at the bottom.

In the light of the background provided by the above-cited literature, we investigate the influence of surface physical and biogeochemical processes on spatial patterns of DPS juvenile and adult abundance using remotely sensed and in situ data, combined with the use of Generalized Additive Modeling (GAM), ocean drifter data and primary production and particle flux models. That is, we investigate the importance of these more "basic" ecological processes in influencing abundance distributions, which are obviously complicated by the more strictly biological factors such as e.g. the food chain zoologically closer to this species, reproductive fecundity, etc.

Considering that larval and early juvenile stages develop in surface waters and knowing that the DPS pelagic stage lasts about 1–2 months (Fortibuoni et al., 2010; Heldt, 1938; Gargano et al., 2022), we applied GAM modeling to identify the relationships between in-situ juvenile DPS abundance and remotely-sensed SST, chlorophyll and their frontal structures with a time-lag of one month. That is, pairing abundances to the above parameters relative to the month before catch. Results show that abundances are sensitive to proximity to SST fronts and high values of chlorophyll front density.

In addition, the analysis of drifter trajectories in the area revealed either recirculation or particle slow-down sites in the proximity of high DPS abundances. This suggested that these sites may be favorable to the foraging of the bottom community, by sinking of POC produced at the surface. Thus, we compare the DPS total (adult and juvenile, caught at the bottom) abundances to those of bottom POC flux, obtained from surface primary production and models of POC sinking, remineralization and horizontal advection-diffusion using model currents of the SoS.

Results indicate a link between DPS juvenile abundance and catch depth, distance from SST fronts and chlorophyll front robustness. Also, a good agreement is found between high POC concentration at the bottom and DPS abundance patterns, but only when both 1-D sinking/remineralization algorithms and horizontal POC diffusion are employed to estimate bottom POC fluxes, given the highly dynamic structure of the SoS circulation.

This work was stimulated by the fact that to improve our understanding of the environmental controls on benthic communities is key to enhance our predictive capabilities in support of fishery management. As there is no simple relationship between surface and bottom dynamics,

this requires a comprehensive assessment of the multiple physical and biogeochemical processes that can impact the distribution of benthic communities and high trophic levels in coastal areas.

2. Materials and methods

2.1. Study area

The study area (Fig. 1) is located in the northern sector of the SoS (south-central Mediterranean Sea) and corresponds to the General Fisheries Commission for the Mediterranean (GFCM) Geographical Sub Area 16 (GSA 16 – South of Sicily; FAO GFCM, 2009). Its continental platform is made of two wide and shallow (<100 m) banks at the western (Adventure Bank - AB in Fig. 1a) and eastern (Malta Plateau - MP in Fig. 1a) boundaries of the Strait, respectively, connected by the narrow Sicilian shelf between them. The banks' margins are steep and incised by many canyons and trenches.

The general circulation pattern is characterized by the eastward flow (0–150 m depth) of relatively fresh Modified Atlantic Water (MAW) entering the study area from the west as the energetic and meandering Atlantic Ionian Stream (AIS in Fig. 1a; e.g. Robinson et al., 1999). The AIS flows into the Strait offshore of Adventure Bank and at times flows close to the southern coast of Sicily or meanders offshore in the middle of the Strait (e.g. as in Fig. 1a). It then reaches the Malta Plateau and the Ionian Sea to the east. Next, the area to the north, between the AIS path and the south Sicilian coast is often subject to upwelling along the latter coast, partly provoked and maintained by frequent and intense winds blowing from the NW-SW sector in the area (e.g. Piccioni et al., 1988; Béranger et al., 2004; Askari, 1998, 2001; see also Fig. 4a below). The main geostrophic upwelling-related current (UC in Fig. 1a) flows southeastwards along the southern Sicilian coast and enters the Ionian Sea as a filament detaching from the southeastern tip of Sicily (Bignami et al., 2008). Also, the UC is subject to instabilities caused by the topography of the Strait, current horizontal shear between the coastal waters and the AIS and stratification. Instabilities include the Adventure Bank Vortex (ABV, cyclonic, Fig. 1a) located in the lee (southeast) of the Adventure Bank, the Ionian Shelf break Vortex (ISV, cyclonic) located over the Malta Plateau (Fig. 1a), off the southeastern coast of Sicily. Finally, an intermittent southward (offshore) branching of the upwelling coastal current occurs from Sicily towards Malta, being ecologically relevant for offshore export of pelagic fish larvae (Fig. 1; Falcini et al., 2015).

2.2. Deep-water rose shrimp abundance data

The DPS abundance data were collected during bottom trawl surveys carried out in the GSA 16 within the MEDITS (MEDiterranean International Bottom Trawl-Surveys; Bertrand et al., 2002) and GRUND (GRUppo Nazionale risorse Demersali, i.e. National Demersal resources Group; Relini, 2000) programs (Fig. 1, Table 1). The data collected in the

Table 1
Start and end dates (day/month) and number of stations of MEDITS (left) and GRUND (right) 1998–2008 trawl surveys.

Surveys	Start - end (dd/mm)	n. sta.	Surveys	Start - end (dd/mm)	n. sta.
MEDITS 1998	16/06–27/06	42	GRUND 1998	01/10–12/12	62
MEDITS 1999	28/05–09/06	42	GRUND 1999	No survey	0
MEDITS 2000	26/05 - 05/06	42	GRUND 2000	30/09–11/11	53
MEDITS 2001	19/05–01/06	42	GRUND 2001	04/09–18/11	53
MEDITS 2002	11/07–04/08	66	GRUND 2002	24/09–07/10	48
MEDITS 2003	13/07–13/08	66	GRUND 2003	12/09–06/11	48
MEDITS 2004	11/06–09/07	65	GRUND 2004	28/09–29/10	47
MEDITS 2005	06/07–11/08	108	GRUND 2005	12/11–23/12	126
MEDITS 2006	20/05–12/06	114	GRUND 2006	14/11–22/12	132
MEDITS 2007	11/06–08/07	120	GRUND 2007	No survey	0
MEDITS 2008	12/05–06/06	120	GRUND 2008	11/10–18/11	151

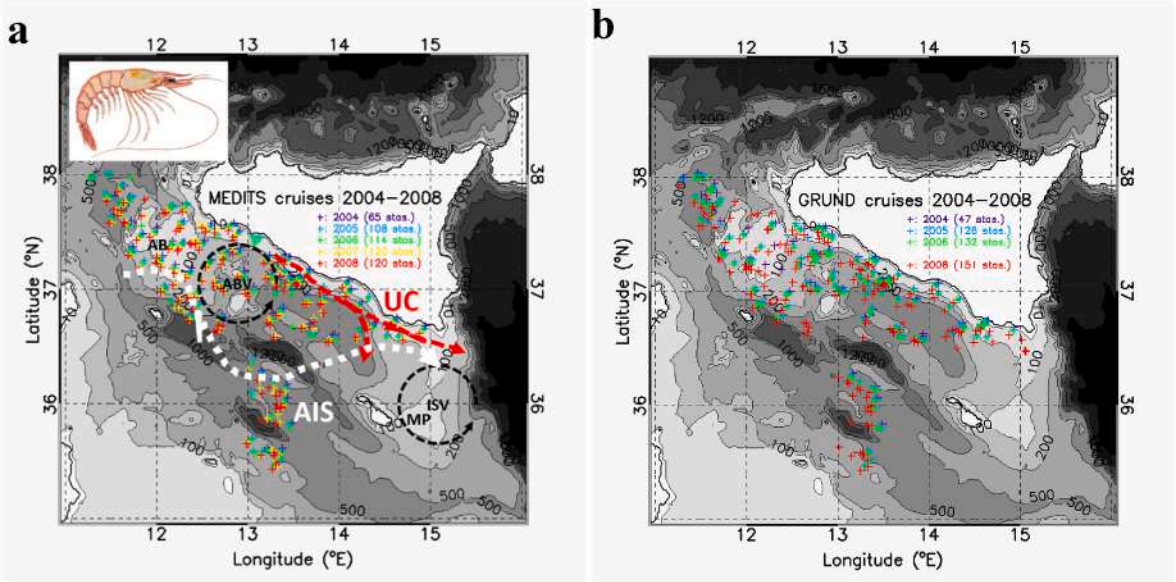

Fig. 1. (a) MEDITS (inset: *P. longirostris*) and (b) GRUND stations in the SoS, for 2004–2008 and bathymetry in meters (grayscale). These are the years of available satellite SST and chlorophyll imagery and frontal products. Sampling stations (crosses) are color-coded for the years as in the legend, which displays also the total number of stations per survey (NOTE: no GRUND trawl survey was carried out in 2007). Panel (a) also includes the Atlantic-Ionian Stream (AIS, dashed white arrow), the Adventure Bank Vortex (ABV, cyclonic), the Ionian Shelf break Vortex (ISV, cyclonic), the upwelling current and its occasional southward branching (UC, dashed red arrows). AB indicates the Adventure Bank, MP the Malta Plateau, less than 100 m deep, in the northwestern and southeastern limits of the Strait of Sicily.

years 2004–2008 were used for the GAM investigation of the relationship with remotely sensed SST and *chl* frontal structures, the latter having been produced for these years only (see Section 2.3 below). Next, the 1998–2005 DPS abundance data were used to investigate the DPS - POC bottom flux relationship, once again because POC calculations were based on surface primary production (PP) maps available only for these years (see Sect. 2.6). We recognize that the GAM and POC analysis DPS data periods do not coincide, but we opted to use the maximum amount of data available in each case, so as to have as robust as possible results for an average/stationary situation.

In Table 1 we present the start/end dates and number of stations of the 1998–2008 cruises analyzed in this work, even though the MEDITS cruise program sampling was carried out in spring/early summer for the 1994–2010 period, while GRUND stations were sampled in autumn in 1990–2008, except for 1999 and 2007.

The MEDITS and GRUND sampling programs employed a random sampling design stratified by depth (depth strata: 10–50 m, 51–100 m, 101–200 m, 201–500 m, 501–800 m). The entire catch of each sampling station was analyzed in terms of number of individuals and weight per species. DPS individuals were weighed, and the carapace length (CL) was measured to the nearest mm. Density indices of DPS per station were expressed as number of individuals per 100 km^2 (indiv./100 km^2), assuming a catchability coefficient equal to 1. Note that the catchabilities of the gears used during the surveys, i.e. the GOC 73 trawl net used for the MEDITS program and the Italian commercial tartana net used for the GRUND sampling are not the same. Therefore, the abundance indices (number of individuals per km^2) from the GRUND surveys were uniformed to those of the MEDITS surveys, by using a fishing power correction factor of 0.84 proposed by Scalisi et al. (1998) for the DPS. To estimate abundance by life phase, juveniles in their first year of life were separated from adults as individuals below 20 mm CL using the standardized length frequency distribution in number of individuals per km^2 according to Colloca et al. (2015).

Average DPS abundances across all the GRUND and MEDITS surveys were mapped. Each map was drawn by gridding (IDL software linear interpolation) the abundance data recorded in the stations of each survey - one MEDITS and one GRUND survey per year - and averaging the yearly grids for each of the two programs. The grid is made of 61 × 49 pixels, each with a linear dimension of 6.4 nautical miles (i.e. approximately 12 km), comparable to the average distance between stations in the original data.

The corresponding abundance variabilities are also given, computed at each grid point *(i,j)* as a proxy of the coefficient of variation among the surveys, i.e.

$$[max(abundance(i,j,t)) - min(abundance(i,j,t))]/<abundance(i,j,t)>,$$

where *t* indicates surveys (i.e. years) and $<>$ indicates the average value over the surveys.

2.3. SST and chlorophyll satellite data

Daily sea surface temperature (SST) data were acquired from the Multi-scale Ultra-high Resolution (MUR) Sea Surface Temperature Analysis Level 3 dataset (https://podaac.jpl.nasa.gov/Multi-scale_Ultra-high_Resolution_MUR-SST). The maps cover the seas around Italy (latitude range: 34° 00.00′ N - 46° 00.00′ N, longitude range: 009° 00.00′ E – 020° 00.00′ E), while we show here only the details of the SoS for our purposes. The spatial resolution of the maps is about 1.1 km, i.e. 1002 × 1094 pixels, and the maps were combined into 8-day median composites for the period 2004–2008. The 8-day span for the composites was chosen after Miller (2009), in order to optimize some of the frontal products described below, which needed multi-day observations, such as front persistence and density.

Surface chlorophyll maps of the same time period and the same spatial and temporal resolution as above were obtained from the MyOcean Level 3 daily surface chlorophyll (SeaWiFS sensor data, MedOC4 algorithm of Volpe et al., 2007) for the Mediterranean Sea (http://marine.copernicus.eu/).

Thermal and chlorophyll ocean fronts were detected on each daily map (Miller, 2009) and used to generate 8-day and monthly ocean front metrics using the method of Miller et al. (2015) and briefly described in Table 2.

2.4. Generalized additive models (GAM)

Generalized additive models (GAM; Wood, 2006) were applied to assess the relationship between abundance of DPS juveniles and monthly averages of SST, *chl* distributions and the frontal parameters cited above, for the period of availability of such frontal products, i.e. 2004-2008. DPS juvenile abundances recorded in the first (second) half of a given month were paired to SST, *chl* and frontal product averages for the previous (current) month, relative to the entire 2004–2008 SST/*chl* frontal dataset period. GAMs use smoothing functions to model nonlinear relationships (Hastie and Tibshirani, 1990) and they were considered appropriate models for our study, due to the unknown form of predictor-response relationships. The density of DPS juveniles in each station was used as the response variable and modeled as a function of the linear combination of smoothers representing the effects of the different oceanographic variables. Initially, depth, SST, and *chl* and all their front metrics (*Fdist*, *Gdens*, *Pfront* and *Fdens*, Table 2) were considered as potential independent variables. However, collinearity among covariates was examined with pair plots and variance inflation factors (VIF), an index which measures how much the variance increases because of correlation between predictor variables. The variables with the highest VIF were iteratively removed until all covariates showed a VIF <2 (Zuur et al., 2007). This caused *Gdens* and *Pfront* for both SST and *chl* to be dropped from the analysis. Data for both surveys (MEDITS and GRUND) were combined in a single data set, and year and season were modeled as factors.

The DPS juvenile density was log-transformed and a GAM with the Gaussian distribution and identity link function was applied. The modeling procedure started by constructing a full model including all the independent variables cited above. Smooth terms were modeled using penalized thin plate regression splines with smoothing parameter selection based on generalized cross-validation (GCV) criteria (Wood, 2006). Inspection of the residual GAM fit using semi-variograms gave an indication of spatial autocorrelation, which generated a violation of the assumption of independence (Zuur et al., 2009). In order to obtain a more robust model accounting for spatial autocorrelation of the residuals, a mixed GAM (GAMM; Zuur et al., 2009) with an exponential spatial correlation structure nested in each season of the year was finally used. The GAMM model is described as follows.

$$g(Y_i) = \alpha + \sum_{k=1}^{n} f_k(x_k) + \varepsilon_i$$

Table 2
SST and chlorophyll front metrics description (Miller et al., 2015).

Metric	Meaning	Method
Fdist – distance to front	Distance of map pixel from the closest major front	Identified using a custom simplification algorithm
Gdens – front gradient density	Local neighborhood average of frontal gradients, avoiding the discrete nature of individual detected front contours	Application of Gaussian smoothing filter (sigma = 5 pixels) to mean gradient map
Pfront – front persistence	Fraction of cloud-free observations of each pixel, for which a front is detected	Count front occurrences plus Gaussian filter smoothing of result
Fdens – front density	Single metric summarizing front gradient, persistence and also proximity to neighboring fronts	Product of front gradient, persistence and proximity values

$$\varepsilon_i \sim \text{Normal}(0,\sigma^2)$$

$$cov(\varepsilon_i, \varepsilon_j) = \begin{cases} 1 \text{ if } i = j \\ 1 - e^{\frac{d}{r}} \text{ else} \end{cases}$$

with $g(Y_i)$ denoting the link function defining the relationship between the response variable Y_i (juvenile abundance) and the additive predictors x_i (e.g. SST, *chl* and frontal parameters). α and $f_k(x_k)$ respectively denote the sought-for intercept and arbitrary smooth function of independent variable x_k. ε_i is a normally-distributed error for Y_i, having zero mean and σ variance. In the covariance model $cov(\varepsilon_i, \varepsilon_j)$, d denotes the maximum separation distance of the residual (observed minus estimated values) spatial position to be considered for the semivariance estimates (depicting the spatial autocorrelation of the residual sample points). r is the distance above which residuals are no longer related (i.e. range). The maximum distance d was found to be 120 Km, one third of the maximum distance between field data.

Model selection was performed using a backward stepwise procedure, by dropping, one by one, from the full model those variables resulting not significant and comparing the nested models (i.e. the simplified model with parameters representing a subset of a complex model) using Akaike's information criterion (AIC) and likelihood ratio test (Zuur et al., 2009). Standard diagnostics plots (Wood, 2006) were used to assess model fit and validity. The GAM(M) was fitted with the *mgcv* package (Wood, 2006) of the R v. 2.14.2 statistical package (R Development Core Team, 2011).

2.5. Lagrangian drifter data

The drifter data we have used to characterize the surface circulation features which could affect DPS abundance in the SoS are part of the Mediterranean Drifter Data Base, which contains the vast majority of near-surface drifters deployed in the last decades in the Mediterranean Sea (see e.g., Zambianchi et al., 2017). The 199 drifters transiting in the SoS and deployed between 1998 and 2005 have been analyzed in this study.

These drifter data are processed and archived by the Istituto Nazionale di Oceanografia e di Geofisica Sperimentale (OGS) in Trieste, Italy (see https://nodc.ogs.it/). Time series of drifter positions in each trajectory were filtered to remove high frequencies and then subsampled every 6 h (see Poulain et al., 2012, for further details about dataset and data treatment).

The drifters we have considered are mainly of two different types: Surface Velocity Program (SVP) and Coastal Ocean Dynamics Experiment (CODE) units. They are all characterized by the presence of a drogue at a certain depth, aimed at maximizing current drag with respect to the surface windage effects. SVPs are equipped with a holey-sock drogue centered at 15 m depth (Lumpkin and Pazos, 2007), while CODE and CODE-modified drifter drogues cover the upper 70 cm to 1 m portion of the water column (Pisano et al., 2016). Therefore, the different drifter types should provide information on the near-surface current flowing at different depths. However, both reference depths are well above the 50 m euphotic zone definition that we used in this work for our model reconstruction, thus we can consider them equivalently describing the near-surface velocity field.

2.6. Primary production (PP) and particulate organic carbon (POC) flux data

We estimated the Particulate Organic Carbon (POC) 8-day mean flux at the sea bottom, as a proxy of organic detritus, in order to compare its spatial pattern to that of shrimp abundance. To do so, we utilized 8-day surface primary production (PP) maps of the Mediterranean Sea for 1998–2005 (unfortunately not available for 2006–2008), produced with the empirical model by Colella (2006). The model by Colella (2006) estimates PP as a function of SST (AVHRR sensor), chlorophyll from satellite data (SeaWiFS, MODIS and MERIS sensors), SeaWiFS Photosynthetically Available Radiation (PAR), and a mixed layer depth (MLD) climatology, the latter to reconstruct subsurface chlorophyll profiles (D'Ortenzio et al., 2005). We acknowledge that the period of the PP and POC data (1998–2005) differs from that of the DPS abundance (1998–2008) and satellite SST/chl frontal products (2004–2008), but the adoption here of a multi-year average for POC calculation somewhat attenuates this problem. This is because of the high stability throughout years of DPS nursery and/or spawning area spatial distributions and of the main features of adult DPS distribution in the SoS (Fortibuoni et al., 2010; Garofalo et al., 2011; Colloca et al., 2015), despite quantitative variations of the latter in the more recent years (Sbrana et al., 2019).

The PP maps were used to estimate the POC fluxes at 50 m, chosen as an approximate euphotic zone limit depth, by applying the 1-D model of Pace et al. (1987; hereafter P87). We adopt this depth as a preliminary, very rough value for the euphotic zone base depth, in the light of typical values of light attenuation coefficient at 490 nm (K490) satellite data of the area.

The POC flux below the euphotic zone as a function of depth z is computed as (P87):

$$POC(z) = 3.523\, z^{0.734}\, PP^{1.000} \left(\text{in mg C m}^{-2}\text{ d}^{-1} \text{ converted to g C m}^{-2}\text{ d}^{-1}\right).$$

This equation is valid below the euphotic zone and was tested by the P87 authors, using in situ datasets of simultaneous PP and POC flux measurements, with uncertainties on the coefficients of about 25%.

We thus obtained 8-day $POC_{50,8d}$ fluxes at 50 m, from the PP maps. The $POC_{50,8d}$ fluxes were then averaged into a single multi-year POC flux map (POC_{50}) covering the 1998–2005 period. Bottom fluxes POC_{btm} were obtained using the bathymetry depths of the area (NRL 5-min bathymetry, see https://cmr.earthdata.nasa.gov/search/concepts/C1214614815-SCIOPS.html) and the P87 algorithm described above.

The sensitivity of POC_{btm} estimates to the type of 1-D algorithm has been somewhat tested by using also the algorithm described in Kriest and Oschlies (2008; hereafter K08), in whose study the POC flux $F(z)$ at a given depth is computed as:

$$F(z) = F(z_0)\left(\frac{z}{z_0}\right)^{-\frac{r}{a}}$$

where z is depth, $z_0 = 50$ m is our euphotic zone base depth, $F(z_0)$ is the POC flux at z_0 (we use our POC_{50}), $r = 0.0302\text{ d}^{-1}$ is the remineralization rate as inferred in K08 and $a = 0.0352\text{ d}^{-1}$ is a parameter derived from organic matter sinking velocity considerations, also described in K08.

These 1-D POC flux algorithms neglect the effect of horizontal advection/diffusion on POC distribution. However, the SoS is a site of strong horizontal currents at all depths (see Sect. 2.1). These include the AIS and the southern Sicilian upwelling system at the surface (e.g. Robinson et al., 1999; Piccioni et al., 1988), the Levantine Intermediate Water layer and the bottom current system, the latter two directed essentially along-strait from the Ionian to the Western Mediterranean Sea (e.g. Astraldi et al., 2001). All these dynamic features may significantly shift POC laterally while sinking, and thus displace the deposition sites relative to the surface productive zones (Siegel and Deuser, 1997).

To account for these horizontal processes, the 1998–2005 average POC_{50} map was fed, as an initial tracer field, to a Crank-Nicholson 2D horizontal advection-diffusion scheme (courtesy of Dr. B. Zhang, National Institute of Aerospace, USA). The code was run using the horizontal current fields generated by the Sicily Channel Regional Model (SCRM) circulation model, a widely validated Princeton Ocean Model (POM) implementation for the SoS Area (Sorgente et al., 2011; Olita et al., 2012; http://www.seaforecast.cnr.it/). A horizontal eddy diffusion coefficient range $10^7 < K_H < 5 \times 10^7\text{ cm}^2\text{ s}^{-1}$, resulting from real drifter data in the area (Poulain and Zambianchi, 2007), was adopted in

the advection/diffusion scheme. These values are of the same order of magnitude of typical K_H values in the ocean (Corrado et al., 2017). Note that K_H has been estimated with surface drifters, but we adopted it throughout the water column in this first approximate study. Even though the Crank-Nicolson scheme is unconditionally stable, the time step Δt for the POC advection/diffusion simulations was conservatively obtained by setting the Courant-Friedrichs-Lewy number of the advection/diffusion scheme $CFL = K_H\ \Delta t/\Delta x^2 = 0.9$, i.e. with the CFL <1 condition for stability in most schemes. This yields $1 < \Delta t < 5.2$ h, given the POC grid resolution $\Delta x = 0.05°$ (5.3 km) and the above K_H range. Δt is computed for each (Δx K_H), couple in the various runs.

The code's flowchart is, for each couple of simulation time steps *i-1* to *i*:

1) the model horizontal current field at depth z_i (to which the POC has sunk) is obtained by linearly interpolating the model current vertical levels just above and below z_i;
2) Δt is computed for the (Δx, K_H) input values and the POC_{i-1} map issuing from the preceding iteration is allowed to diffuse-advect horizontally for a time Δt, using the above current field, thus obtaining a first version of POC_i, not yet attenuated;
3) POC_i is then attenuated as $POC_i = POC_{i-1} \times (z_i/z_{i-1})^{-0.734}$, following P87, or $POC_i = POC_{i-1}$ (1 - $R \times \Delta t$) in runs using K08;
4) all POC_i pixels which have touched bottom (i.e. where z_i greater or equal local bathymetry) are removed from the POC_i map and added to an initially empty bottom POC flux map, POC_{btm}, which is our output at the end of the simulation;
5) the depth z_{i+1} of the next POC_{i+1} map is calculated as $z_{i+1} = z_i + v_{sink} \times \Delta t$, with a constant v_{sink} introduced for the P87 algorithm or the depth-dependent $v_{sink} = 0.0352\ z$ m d^{-1} for the K08 algorithm;
6) repeat from item 1).

The algorithm stops at a given step *i* when z_i of the sinking POC field is greater than the deepest bathymetry value of the study area, or when POC has decreased to practically near-zero, i.e. when $max(POC_i) < 10^{-5}$

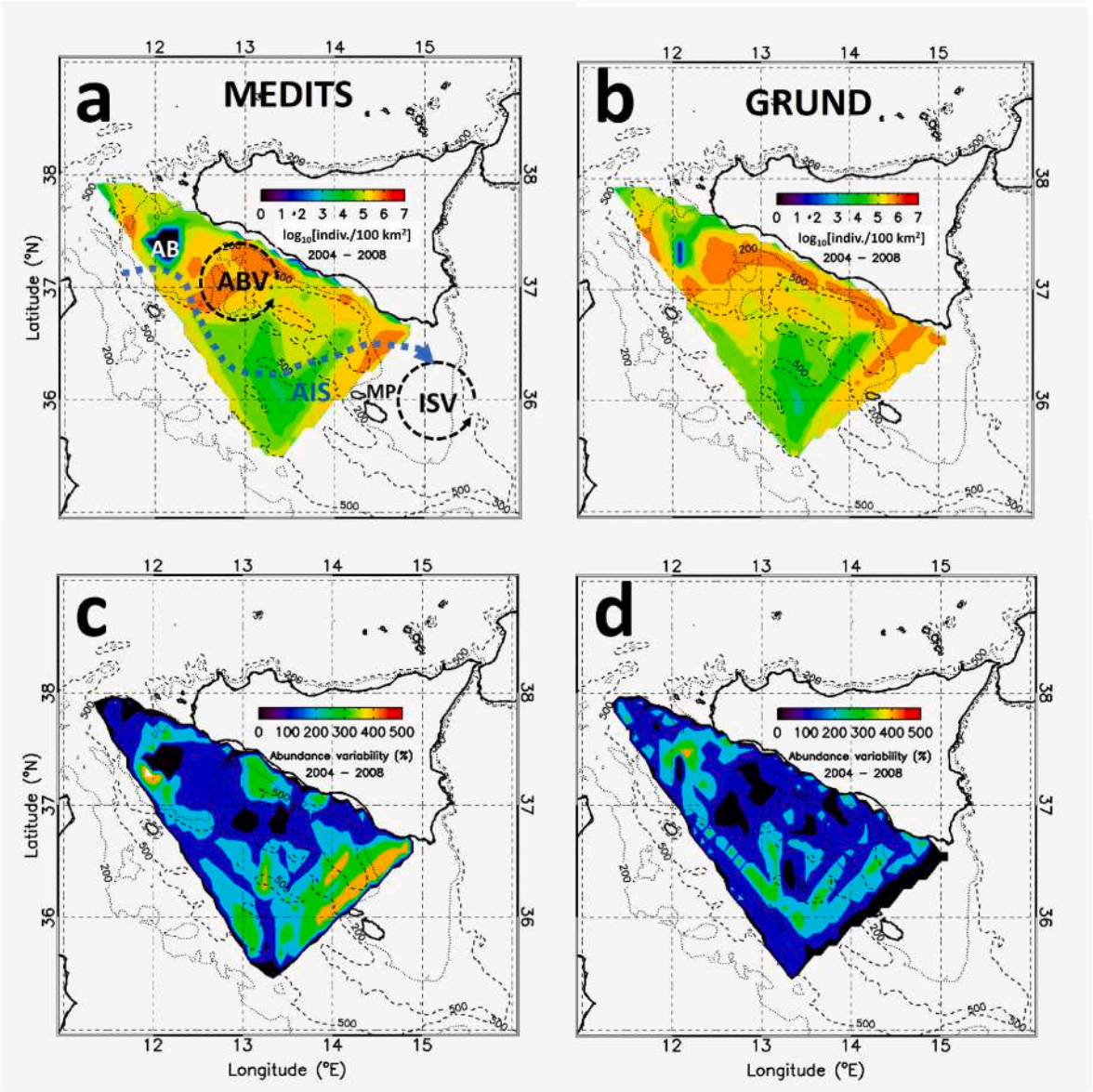

Fig. 2. Average rose shrimp abundance in $\log_{10}$ (indiv./100 km^2), overplotted on bathymetry, for the (a) MEDITS and (b) GRUND surveys of 2004–2008, and abundance variability (see Section 2.2) for (c) MEDITS and (d) GRUND 2004–2008. Regions that have never been sampled are in white. Panel (a) also includes schematic locations of the Atlantic-Ionian Stream (AIS, blue curve), Adventure Bank vortex (ABV, cyclonic) and Ionian Shelf-break Vortex (ISV, cyclonic).

g C m^{-2} d^{-1}.

Note that the POC_{50} data are in g C d^{-1} m^{-2}, so our simulations treat a one-day POC_{50} flux impulse issuing from the euphotic zone and reaching the bottom. Therefore, the simulation results discussed below do NOT give a measure of POC_{btm} (e.g. multi-year) accumulation at the bottom, but only reveal where surface-produced POC may be deposited at the bottom. A very rough bottom POC accumulation estimate is obtained by multiplying the obtained constant POC_{btm} by the number of days of a given period of interest.

3. Results and discussion

3.1. Spatial patterns of deep-water rose shrimp abundance

The highest DPS abundances (orange hues in Fig. 2a and b) are on the slopes of the Adventure Bank (AB in Fig. 2a), in the northwestern portion of the Strait of Sicily, and along the southeastern coast of Sicily. Moreover, high abundances approximately coincide spatially with low interannual abundance variability, both for the MEDITS and the GRUND programs (Fig. 2c and d), thus suggesting a rather stable spatial distribution. We add that these average patterns are quite independent of the time series length. Indeed, as a "stability" test, we also computed the averages for a longer period for which both GRUND and MEDITS data were available to us, i.e. 1994-2008 (not shown), and we remark that the average distribution is much the same as for 2004–2008 shown Fig. 2a and b.

However, for completeness, we must cite the fact that changes in DPS abundance in terms of individuals per unit area have been relevant in the years subsequent to those of the data presented here, as shown in Sbrana et al. (2019, see their Fig. 3). Nevertheless, the same figure shows that the main geographic patterns of DPS distribution have remained similar. Therefore, the reader may consider this study as a conceptual and somewhat novel approach to identify the natural forcing of such distributions, applicable to and to be verified with more recent datasets, once the data types used here are available for other time periods.

Despite the observed constancy of the distribution patterns, some differences can be noted between MEDITS and GRUND abundance averages, the cruises being carried out in May–July and September–December, respectively (compare Fig. 2a with b). That is, the highest DPS abundances just east of Adventure Bank are deeper and more to the east in the MEDITS spring-summer (Fig. 2a) than in the GRUND fall-winter surveys. (Fig. 2b).

These spatial patterns are consistent with findings of earlier studies, which investigated the location and persistence of spawning and/or nursery areas of DPS over the period 1994–2004 (Fortibuoni et al., 2010; Garofalo et al., 2011) and nurseries from 1994 to 2010 (Colloca et al., 2015). The above authors observed a rather stable spatial pattern for locations of high young-of-the-year and mature female DPS abundances. According to Fortibuoni et al. (2010) these high abundance regions extended towards deeper bottom depths during spring, in the Adventure Bank Vortex (ABV) region, where we find high DPS abundance (Fig. 2a and b).

The distribution of sampling stations vs. bottom (i.e. trawl) depth is presented in Fig. 3a, b and DPS abundance vs. depth is shown in Fig. 3c, d for 2004–2008. The latter show the wide depth range occupied by the species (about 30–700 m), with higher abundances at shallower depths during fall-winter (GRUND, Fig. 3d) compared to summer surveys (MEDITS, Fig. 3c), as noted in Fig. 2 above. Also, Fig. 3c, d qualitatively anticipate the GAM results illustrated below, in that the juvenile portions of the total abundances, represented by the grey parts of each histogram bar, are always higher for the (shallower) 40–200 m trawl depth range.

3.2. DPS abundance, remotely sensed parameters and GAM(M) results

Fig. 4 exemplifies the 8-day mean SST (Fig. 4a) and surface chlorophyll (Fig. 4b) distributions and the corresponding frontal analysis data (Fig. 4c–h), relative to Oct. 15–22, 2004, i.e. during the 2004 GRUND cruise. Red crosses and triangles indicate DPS abundance measured in the stations of those days, respectively for abundances with more or less than 50% juveniles in the catch of the station.

The cold feature (blue hues) between the AIS and the southern

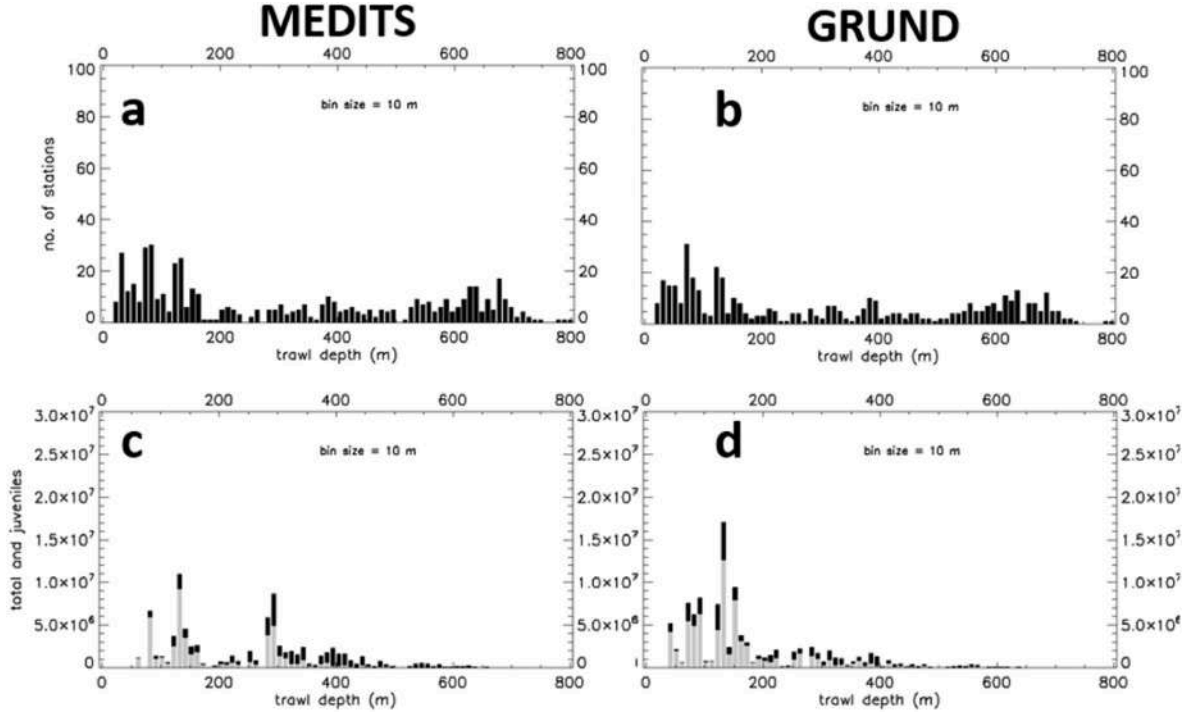

Fig. 3. (a) MEDITS and (b) GRUND 2004–2008 survey station distribution vs. bottom depth; (c, d) 2004–2008 cumulative DPS abundance vs. depth. Total abundance (in indiv./100 km^2) is the total height of each histogram bar in panels (c) and (d) (grey plus black bar), while grey bars indicate juvenile abundances.

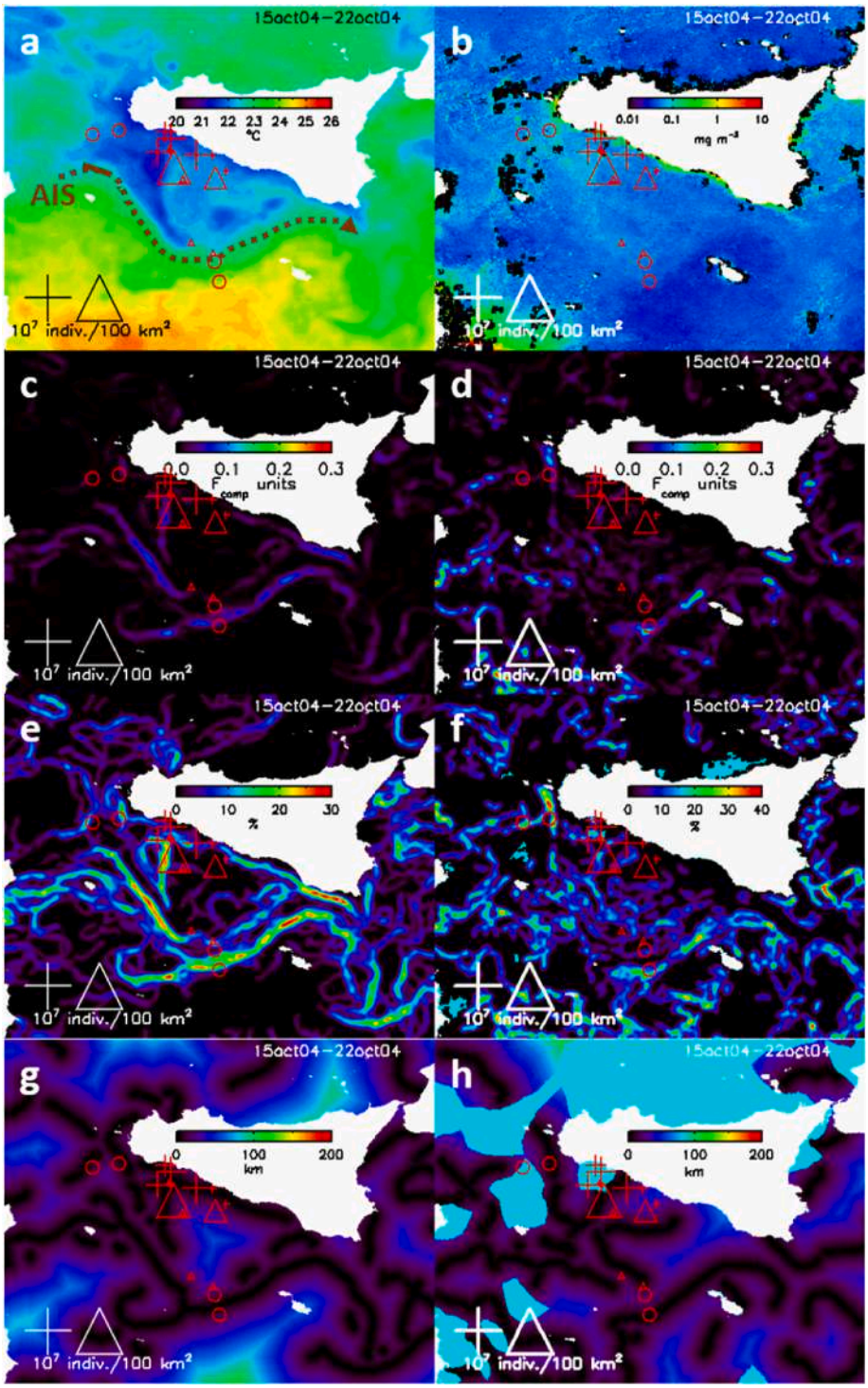

Fig. 4. 8-day mean maps of satellite data, relative to Oct. 15–22 2004, with DPS abundances (indiv./100 km^2) from the corresponding GRUND survey (Sep. 28 - Oct. 29, 2004). Red crosses (triangles) indicate abundance with more (less) than 50% juveniles in the catch of the station. Red circles indicate zero abundance. Abundance symbol sizes are proportional to the $\log_{10}$ (indiv./100 km^2) in each station; the legend at lower left exemplifies symbol size for an abundance of 10^7 indiv./100 km^2. (a) MUR SST (in °C; the brown dotted curve is the AIS, the colder features north of the AIS are upwelling waters); (b) MODIS *chl* (mg m^{-3}); (c) and (d) SST and *chl* front density *Fdens* (F_{comp} units); (e) and (f) SST and *chl* front probability *Pfront* (%); (g) and (h) *Fdist* distance to closest major SST and *chl* front (km) (light blue areas: missing data due to cloud cover).

Sicilian coast (Fig. 4a) is due to coastal upwelling, reinforced by the frequent local winds blowing from the NW-SW sector (Piccioni et al., 1988). The waters at 22–23 °C, located south of the cold waters of the upwelling zone, highlight the typical meandering of the AIS (Fig. 4a, dashed line; Lermusiaux and Robinson, 2001; Robinson et al., 1999). Finally, the cold upwelling waters off the southeastern tip of Sicily leave the coast as a cold southward filament and flow into the Ionian Sea (Fig. 4a; Bignami et al., 2008).

All the above low SST features match spatially with relatively high *chl* values, in that the AIS meander (Fig. 4a) seems to be of the same shape and in the same location of the southern boundary of a relatively higher *chl* region lying between the AIS and the coast (Fig. 4b). This

higher *chl* is a typical consequence of the enhanced surface primary production, related to upwelling, in the northern sector of the SoS.

The AIS meander is consequently well evidenced also in the form of the curve of an SST front density *Fdens* maximum in the middle of the Strait (Fig. 4c, blue-purple lines), while the *chl* front is more uncertainly marked, i.e. presents high *Fdens* values only the easternmost half of the SST front meander (Fig. 4d). Indeed, interestingly no *chl* high *Fdens* feature follows the westernmost AIS portion. The absence of a *chl* high *Fdens* signature in the western part of the Strait possibly indicates a southward dispersion of chlorophyll from the Sicilian upwelling zone, across the AIS. Or, alternatively, there is no *chl* front in the west because of the merging of similar chlorophyll contributions from the south Sicilian and Tunisian coastal productive areas, which are closer to each other than the Sicilian and Libyan coasts more to the east (Rinaldi et al., 2014). Consistent with the picture described above, the front probability *Pfront* maps of Fig. 4e, f also show that the AIS *chl* front is persistent only in correspondence of the eastern half of the SST front high-probability (AIS) meander.

Finally, in Fig. 4g, h we give an example of distance-to-closest-front *Fdist* maps, in which each pixel has the value in km of its distance to the closest major front, with 0 km values obviously matching the locations of the fronts presented above.

The DPS abundance data in Fig. 4 also exemplify the frequent occurrence of small nonzero abundances located in both the upwelling zone and all the way offshore to the south, at the AIS border, the latter abundances being represented by the small (low catch) triangles in all Fig. 4 panels. This suggests that the upwelling waters' offshore dispersal may also affect the DPS distribution, via offshore dispersion of individuals. Indeed, the pelagic community has already been seen to be importantly influenced by the above migration, as revealed e.g. in the study of Falcini et al. (2015), relative to anchovy larvae. Also, the role of the current in the larval dispersal of DPS on the SoS was recently investigated by Gargano et al. (2022). By applying a backward-in-time Lagrangian dispersion models to assess where the juveniles recruiting in the nurseries distributed in the northern sector of the SoS come from, the latter Authors confirmed the expected downstream connectivity between spawning and nursery grounds along the Sicilian–Maltese shelf, while a minor and time-varying contribution is due to potential spawning areas identified off the African coast.

Depth, distance from the SST front *Fdist*, intensity of *chl* front *Fdens* and year were the covariates retained in the best GAMM model influencing the log-transformed abundance of DPS juveniles, obtained by a stepwise procedure (Table 3). The adjusted R^2 coefficient of the best model was 0.80. We remind that DPS juvenile abundances of the first (second) half of a month were paired to the frontal product averages of the previous (current) month, for 2004–2008. That is, we hypothesize that the fifteen days previous to the catch influenced the abundance.

The comparison between the performance of the GAMM and the corresponding GAM with the same fixed-effects covariates is shown in Table 3, considering both the full model and the selected best model. The calculation of the deviance explained was possible only for the GAM model with the same fixed-effects covariates (Zuur et al., 2009) and it resulted to be 80.60 % for the selected best model. The results obtained from the covariance model show that data were correlated for distances less than 7 km.

Fig. 5 shows the plots of the partial effects of the predictive variables on the abundance of DPS juveniles. Depth down to 300 m was preferred by juvenile DPS, which reached the maximum abundance between 150 and 250 m (Fig. 5a), as anticipated in the previous section (Fig. 3c and d). Abundance was negatively correlated to depth for greater values of the latter, again quantitatively confirming the juveniles' preference for shallower depths seen in Fig. 3c and d. Next, the effect of SST *Fdist* was linear and positive for fronts closer than ca. 15 km while greater distances from SST fronts negatively affected the juvenile abundance, and the effect became not significant beyond about 30–40 km (Fig. 5b). Next, a non-linear effect of *chl Fdens* on juvenile abundance was found (Fig. 5c). Low values of *chl Fdens* negatively affect abundances, while this effect turned to positive at ca. *chl Fdens* = 0.007 and increased up to ca. 0.08. Above this value, the correlation becomes not significant (Fig. 5c). Finally, the season was not a significant factor, whereas a significant inter-annual variability of juvenile DPS abundance was observed (Fig. 5d). More specifically, abundance decreased until 2007, when it reached its minimum value, and rose again in 2008.

In summary, our results show that depth has a significant impact on the juvenile abundance, with numbers decreasing sharply by around 60,000 at depths of approximately 130 m and reaching near-zero levels around 500 m, suggesting a strong correlation between DPS and depth. However, the model also emphasizes the importance of proximity to SST fronts and areas with high values of chlorophyll front density (*Fdens*) for juvenile DPS. While these factors have a less pronounced effect than depth, they still significantly contribute to high juvenile densities. Indeed, hydrographic fronts are known to act as processes of mechanical retention of fish larvae (Munk et al., 1999) and accumulation of zooplankton (Agostini and Bakun, 2002), so this may also apply to (pelagic) DPS larvae which may benefit of an expected increase of prey availability in frontal zones, thus improving their feeding and growth. These favorable feeding conditions may also affect DPS early juveniles, which adopt vertical migration for feeding (Marin, 2009). Indeed, zooplankton is normally included in the DPS diet even if it is a secondary food item (Mori et al., 2000; Kapiris 2004). A large contribution of zooplankton to the diet of DPS juveniles was found e.g. off the Algerian coast (Nouar et al., 2011), with an increase of micro- and mesoplankton preys observed during periods of high surface production linked to the strong presence of mesoscale eddies in the area. Actually, fronts affect distribution patterns of marine organisms at all trophic levels (Alemany et al., 2014). In particular, the positive association between demersal resources and semi-permanent frontal structures has been recently documented in the southwestern Atlantic Ocean (Alemany et al., 2014). However, this relationship is more intense when the trophic level of the target species or the size of the individuals is smaller (Alemany et al., 2014, 2018). For instance, Alemany et al. (2018) found that smaller fish (juveniles) of a demersal species (*Macruronus magellanicus*), preying

Table 3
Goodness of fit of GAM and GAMM with exponential correlation structure (Cor. Exp.) for both the full model and the selected best model, *s* indicates a thin plate regression spline smoothing function. Parameters are: number of samples (*n*), degrees of freedom (*df*), Akaike's information criterion (*AIC*) value, Log-likelihood ratio test (*L. Ratio*), significance (*p*) and percentage of deviance explained (*Deviance %*).

Model		n	df	AIC	L.Ratio	p	Deviance %
Full	***ln(YoY abundance+1) ~ s(depth) + s(SST_Fdist) + s(SST_Fdens) + s(chl_Fdist) + +s(chl_Fdens) + as.factor(year) + s(SST) + s(chl)+ ε***						
	GAM	649	21	2408.07			81.60
	GAMM (Cor. Exp.)	649	22	2312.64	98.42	<0.0001	
Selected	***ln(YoY abundance+1) ~ s(depth) + s(SST_Fdist) + s(chl_Fdens) + as.factor(year)+ ε***						
	GAM	649	12	2394.01			80.60
	GAMM (Cor. Exp.)	649	13	2286.57	109.88	<0.0001	

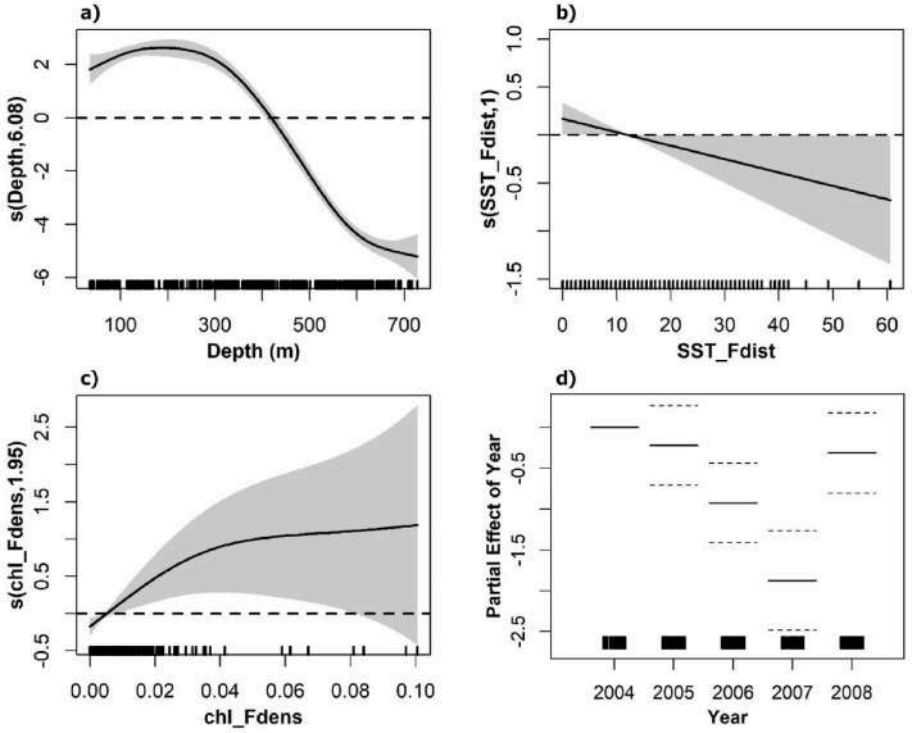

Fig. 5. Partial plot of the best GAMM model. Each plot represents the derived effect of the predictive variables on the DPS juvenile abundance. The number in parentheses indicates the estimated degrees of freedom for the model term (i.e. the amount of the basis function complexity used in the smoothing). Grey areas indicate the 95% confidence interval. Data point densities are shown on the lower axis as a rug plot. (a) Trawl depth; (b) distance to closest SST front (SST_*Fdist*); (c) chl front density (*chl_Fdens*); (d) cruise year.

upon zooplankton, were frequently located along frontal areas on the southern Patagonian shelf. This positive relationship was probably related to the trophic level of juveniles being lower than that of adults. Also, in the Mediterranean Sea individuals of first-year European hake (*Merluccius merluccius*) were preferably located where productive fronts frequently occur near the shelf break (Druon et al., 2015).

3.3. Deep-water rose shrimp abundance and bottom POC flux

Numerous studies find correlations between oceanographic surface parameters and demersal/benthic species abundances (e.g. Sbrana et al., 2019 and references therein). Some of these studies treat the effects of the transmission of the surface physical and biological signal to the benthic community. These studies are not numerous, in that the practical realization of this analysis is extremely costly, in terms of instrumental and human effort. The contemporaneous observation of the sea by means of remote sensing platforms, surface in situ surveys and water column and sea bottom instrumentation (e.g. CTD, sediment traps, biological sampling, etc.) is a tremendous challenge, as may be easily inferred from studies such as that of Rowe and Mahlon (2008) and companion papers. Therefore, given that lack of contemporaneous observations in the region of interest, we made a preliminary somewhat "remote" attempt to investigate the possible links between DPS abundance at the bottom of the SoS and foraging of the latter habitat by surface dynamics and biological production, based on the available data discussed below. This attempt by no means negates the importance of the influence on DPS distribution of deep or bottom environmental parameters, such as oxygen availability for respiration or turbidity conditioning e.g. predation success. However, unfortunately these data sets are sparse. Anyway, where available, they could be the object of more punctual and exhaustive studies, possibly also by means of dedicated research cruises.

Our first step was to analyze a set of 199 drifter trajectories transiting in the Strait during 1998–2005, to infer mean horizontal surface transport and possible accumulation/stagnation sites of biological scalars. This was done in the light of recent investigations aimed at evaluating the importance of the various drivers of biological community dynamics (Cianelli et al., 2017) and partly following the ocean triad concept of Bakun (1998). This is because these stagnation sites could forage the benthic community via organic particle sinking without lateral dispersal.

Single-drifter trajectories were considered, as well as a multi-drifter statistical analysis, given the probably long-time scales with which surface waters may influence the bottom community. Fig. 6a shows a drifter entering the SoS from the northwest, transiting on the Adventure Bank and slowing down close to the Sicilian coast, while describing a circular anticyclonic motion, as highlighted by the blue circle in the figure. The drifter's slowdown is conveyed to the reader in the form of the trajectory's data points being closer together in space, since they are separated by a constant time interval. Next, the drifter describes another closed path more to the southeast and finally exits the Strait off Cape Passero (SE tip of Sicily), into the Ionian Sea. The closed portion of the trajectory in Fig. 6a is located over high DPS abundance (inset in Fig. 6). This indicates that surface biological material produced over Adventure Bank (see *chl* in Fig. 4b) may well transit to the high DPS abundance area and sink there, due to the observed recirculation.

The drifter slowdown in the blue circle sub-area of Fig. 6a is also evident in the spatial distribution of the average drifter residence time in Fig. 6b, computed over all drifters transiting in each of the colored rectangles in the figure. The figure indeed indicates a relative maximum of about 10–20 days close to the recirculation site (green square, close to the coast). The relatively low velocities and therefore longer transit times in most drifter data from the SoS are also clearly shown in the results of Poulain and Zambianchi (2007), relative to the near-surface circulation observed in the 1990s. The authors find that the mean kinetic energy of the flow in the area highlighted in Fig. 6 is the lowest of

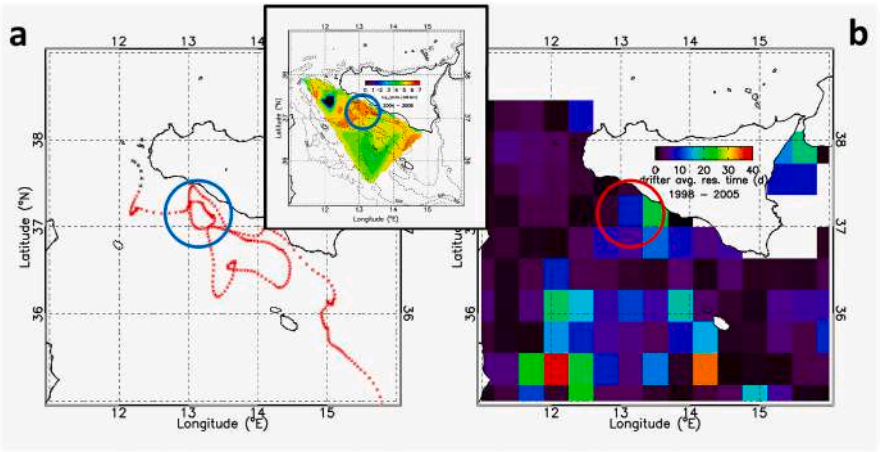

Fig. 6. (a) Trajectory of drifter no. b29300, deployed Feb. 16, 1998, 11:24 UTC, whose last transmission was recorded on Jul. 27, 1998 06:01 UTC. The blue circle evidences the inshore recirculating portion of the trajectory; black asterisks indicate deployment site and first few data points. Inset: 2004–2008 average shrimp abundances of Fig. 2a. (b) Residence time (days) in each rectangular 0.5 × 0.5-degree box, for all 199 drifters deployed in 1998–2005 and transiting in the Strait of Sicily.

that sector of the Strait, thus yielding its largest eddy/mean kinetic energy ratio (see their Fig. 6a and c). Also, the immediate connection between surface waters of this area and those of the Adventure Bank located upstream was seen to be strongly dependent on prevailing winds, and in particular favored by the northwesterly wind regime, which is the most frequent in the area of the Straits (Poulain and Zambianchi, 2007). Finally, our 199-drifter dataset indicates that 30 out of the 60 drifters transiting over Adventure Bank reach the recirculation area or its vicinity, 11 of them transit through the circled area of Fig. 6 and slow down, and 5 of these recirculate similarly to the drifter of Fig. 6a.

The observed recirculation in the high DPS abundance area and the general southeastward flow (not shown) from the highly productive Adventure Bank towards the Ionian Sea, suggested to analyze bottom foraging of Particulate Organic Carbon (POC) produced at the surface and reaching the bottom while re-mineralizing and undergoing horizontal advection-diffusion. This effort was carried out with the modeling tools described in Section 2 and was inspired by the study of Biggs et al. (2008) relative to the remarkably complete Deep Gulf of Mexico Benthos Program (see Rowe and Mahlon, 2008 and companion papers). These authors find that surface POC sinking to the bottom is indeed significant, if not crucial, in foraging the benthic community.

Fig. 7a shows the 1998–2005 average daily POC flux at the base of the euphotic zone (POC_{50}), computed from surface primary production maps (Colella, 2006; see Sect. 2.6) and using the Pace et al. (1987), i.e. P87, remineralization algorithm at 50 m (see Sect. 2.2). POC_{50} constitutes the initial input field to the simulations of POC re-mineralization and sinking and lateral advection/diffusion, described in Section 2.4 above.

The average bottom daily POC_{btm} fluxes resulting from a first 1-D study, i.e. with no horizontal advection/diffusion, are shown in Fig. 7b and c. These POC_{btm} fields are computed using the P87 depth-dependent formula and the K08 (v_{sink}, R) algorithm, respectively. It is encouraging to note that these two independent models yield very similar results, which fact suggests the results' robustness, thus somewhat mutually validating the models. Indeed, percentage differences (not shown) reach at most about 20% between P87 and K08 and this occurring in the deeper portions of the area.

The comparison of shrimp abundance (Fig. 2a and b) to 1-D POC_{btm} distribution suggests only very partial superposition of DPS high abundance and POC_{btm} high values. Indeed, the highest POC_{btm} flux occurs at shallower depths, e.g. over Adventure Bank, where DPS abundances are low on the Bank center, thus revealing lack of spatial correlation between DPS and 1-D POC fluxes. Nevertheless, in both models the small, isolated POC_{btm} maxima located east of Adventure Bank (dashed red circle in Fig. 7b and c) are very close to the persistent spawning and nursery areas (Fig. 7d; see also Giannoulaki et al., 2013). This may point to a trophic relationship between DPS early life stages and POC_{btm}, in the nursery areas.

On the other hand, the match between DPS abundance and some of the POC_{btm} distributions resulting from the 1-D algorithms combined with horizontal advection-diffusion seems more promising, though in need of parameter tuning and experimental confirmation. The latter concept is exemplified in Fig. 8, which shows POC_{btm} obtained by letting the 1998–2005 average POC flux at 50 m (POC_{50}), sink and re-mineralize with the P87 algorithm and diffuse/advect horizontally with the Sicily Strait 2008–2010 averages of the depth-dependent horizontal currents. The computational flowchart was described in Section 2.6 above.

The modeled POC flux appears very sensitive to sinking velocity v_{sink} and horizontal diffusion coefficient K_H (Fig. 8). Fig. 8a–c shows that as K_H increases POC_{btm} decreases. This is possibly because a stronger diffusion spreads, and thus thins out, the initial POC_{50} field, also "smearing" the initial maxima visible in Fig. 7a, in correspondence of the upwelling zone. Therefore, as K_H increases: (1) less POC deposits at the shallow depths where the POC_{50} maxima are located, because it is more rapidly diffused to locations with greater depths and (2) the diffused POC cannot reach the bottom at the latter deeper sites, because of a longer action of remineralization occurring through a deeper water column as it falls to the bottom.

Next, the role of v_{sink} is inferable by comparing Fig. 8a and d and the other analogous figure couples with same K_H and different v_{sink}. These show that when v_{sink} is increased - in our case from 2 to 5 m d^{-1} - more POC reaches the bottom, occupying deeper sites. This is because a faster transit through the water column limits in time horizontal diffusion, and thus the above smearing of the POC maxima, as the POC sinks (remineralization is unaffected by v_{sink} in our parametrization).

Therefore, the simulation that delivers most of the POC_{btm} to the high shrimp abundance zones of Fig. 2a, b is the one with lowest K_H, i.e. 10^7 cm^2 s^{-1} and fastest v_{sink}, i.e. 5 m d^{-1} (Fig. 8d). The fluxes range between 10^{-4} and 10^{-2} g C m^{-2} d^{-1}. Interestingly, this flux range is comparable to that observed in the Gulf of Mexico (circa 4–38 10^{-3} g C m^{-2} d^{-1}; Biggs et al., 2008, see their Table 3), where POC flux spatial variability has been experimentally proven to affect the spatial distribution of the benthic communities. However, the uncertainty in K_H and v_{sink} used in the SoS calls for thorough verification with an in-situ study and constitute a caveat for the use of modeling tools in such process studies.

We also show for completeness (Fig. 9) the simulations using the

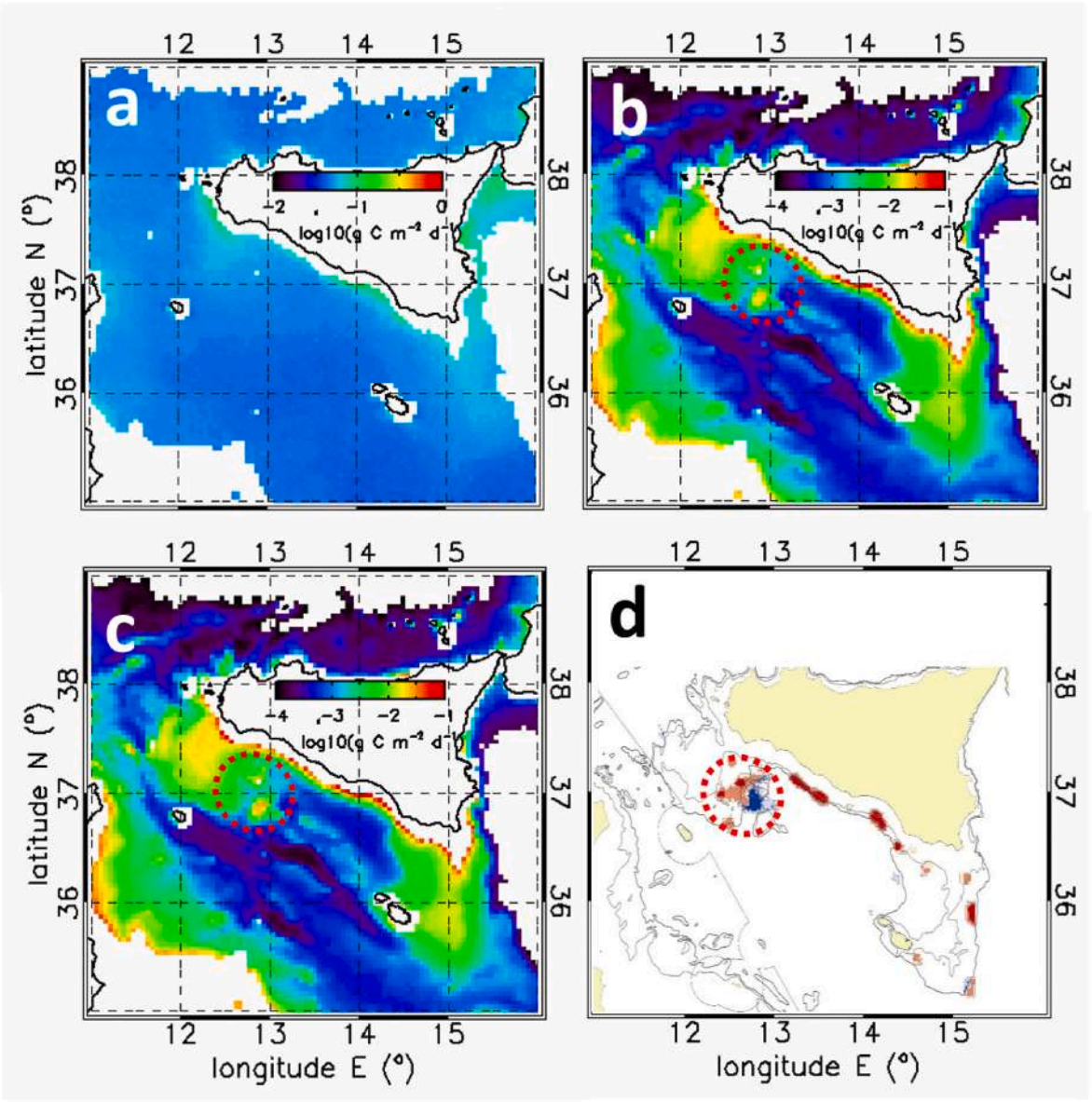

Fig. 7. (a) average POC_{50} at 50 m for 1998–2005 computed from PP maps, via the 1D P87 model (base-10 logarithm of the POC in g C m^{-2} d^{-1}); (b) average bottom POC flux, POC_{btm}, 1998–2005, 1D P87 model (white areas indicate $POC_{btm} = 0$); (c) same as in (b) but computed with the 1D K08 model; (d) In blue: persistent DPS spawning areas; in red and pink: persistent nursery areas. The dashed red circle in Fig. 7b, c indicates POC_{btm} high close to such areas. Please note the different POC flux range in panel (a) with respect to (b) and (c), adopted for graphic clarity.

same horizontal advection/diffusion scheme but coupled to the K08 remineralization R and depth-dependent sinking velocity scheme ($v_{sink} = 0.0352\ z$ m d^{-1}), instead of P87 with constant v_{sink}. Results are conceptually similar to those in Fig. 8, ie., as K_H increases (Fig. 9a–c) POC_{btm} is more localized at the sea bottom beneath high initial POC_{50} areas. We also see that the ($v_{sink}(z)$, R) model of K08 increases POC_{btm} with respect to simulations with P87 (compare Fig. 9 to each row of Fig. 8). This is because $v_{sink}(z)$ becomes much higher than in the fixed case, inducing less diffusion as POC sinks.

Fig. 10 shows histograms of DPS abundance vs. POC_{btm} for the MEDITS and GRUND programs, for the most "favorable" simulation cases, i.e. in which nonzero POC_{btm} is the most spatially widespread. These are the cases of Fig. 8d (P87 model, $K_H = 10^7$ cm^2 s^{-1}, $v_{sink} = 5$ m d^{-1}) and 9a (K08 model, $K_H = 10^7$ cm^2 s^{-1}, variable v_{sink}) and are reproduced as insets in Fig. 10a and c.

The histograms of Fig. 10 confirm that most of the DPS is located where POC_{btm} is in the 10^{-5} - 10^{-2} g C m^{-2} d^{-1} range. In addition, the histograms qualitatively suggest that juveniles are often more present where POC_{btm} has higher values, again possibly indicating that they are trophically closer to POC benthic direct consumers. E.g. the juvenile (grey) portion of histogram bars seem to be greater for POC_{btm} approximately in the 10^{-4} - 10^{-2} g C m^{-2} d^{-1} range in Fig. 10a–c, though not in Fig. 10d. Moreover, a high quantity of DPS is present at very low POC values in Fig. 10b and c. Therefore, a more quantitative analysis is needed, e.g. once the issues relative to model parameter choice (e.g. v_{sink}, K_H) have been better addressed.

It is worth noting that the POC_{btm} spatial distribution does not change much with respect to the shown simulations, when one uses temporally different horizontal current fields or euphotic zone POC_{50} fields, such as daily snapshots. This results from additional runs (not shown) carried out using horizontal currents relative to Feb. 14 and Jul. 14, 2001, coupled with POC_{50} obtained from the corresponding weekly primary production maps.

Our results confirm the major role of the POC flux to the bottom in

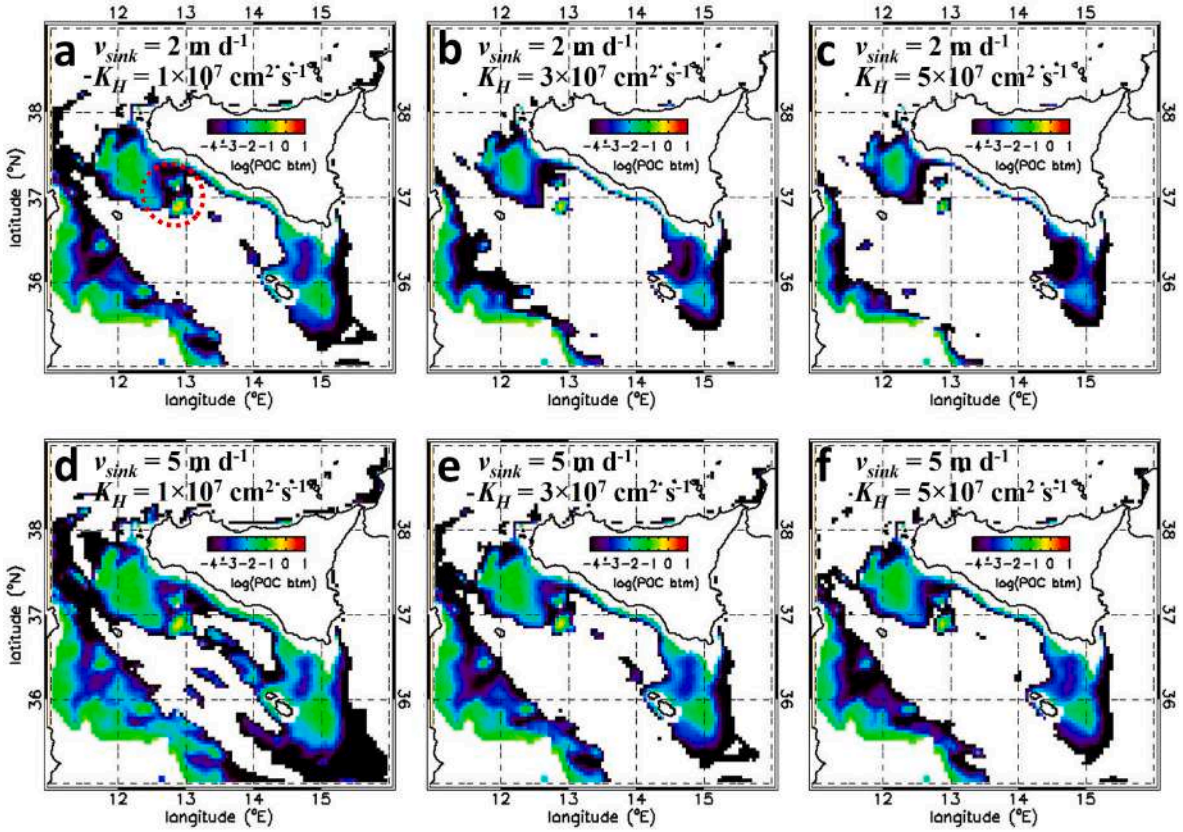

Fig. 8. POC_{btm} (base-10 log of POC in g C m^{-2} d^{-1}) obtained from the sinking and advection of POC_{50} (1998–2005 average) using the P87 1D re-mineralization algorithm coupled with the Strait of Sicily horizontal current 3D model field (2008–2010 average). Panels (a)–(d) show different realizations of POC_{btm} for horizontal diffusion coefficient values $K_H = 1 \times 10^7$, 3×10^7 and 5×10^7 cm^2 s^{-1} (left to right in each row) and for $v_{sink} = 2$ m d^{-1} and $v_{sink} = 5$ m d^{-1} (top to bottom, in each column). The dashed red circle in panel a indicates POC_{btm} high close to nurseries, as in Fig. 7.

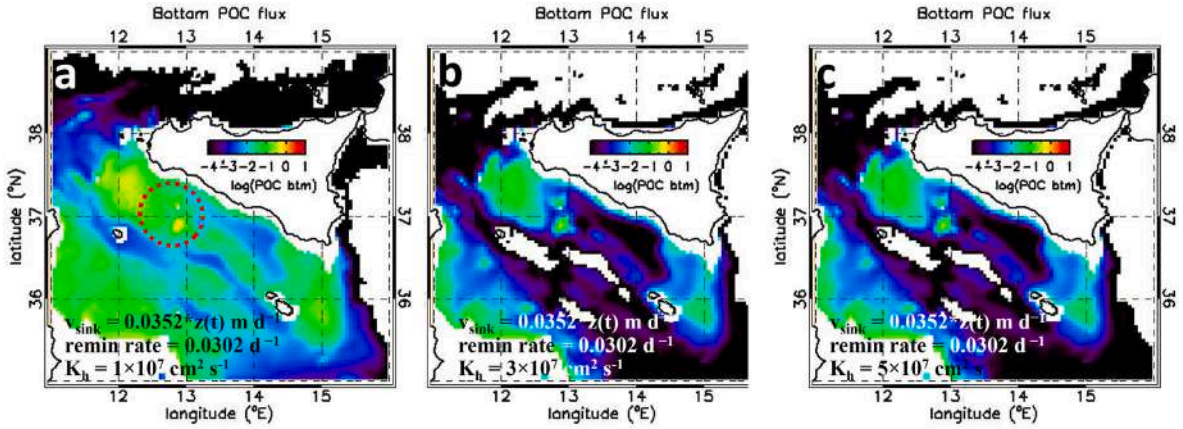

Fig. 9. POC_{btm} (base-10 log of POC in g C m^{-2} d^{-1}) obtained from the sinking and advection of POC_{50} (1998–2005 average) using the K08 1D sinking and re-mineralization algorithm ($v_{sink}(z)$, R) and the 2008–2010 average horizontal model current field. Panels (a)–(c) show different realizations of POC_{btm} for horizontal diffusion coefficient values $K_H = 10^7$, 3×10^7 and 5×10^7 cm^2 s^{-1} (left to right). The dashed red circle in panel a indicates POC_{btm} high close to nurseries, as in Fig. 7.

the benthic-pelagic coupling within the trophic web, as described in general by Tecchio et al. (2015) for Mediterranean deep-sea ecosystems and in particular by Agnetta et al. (2019) for the SoS.

4. Conclusions

This study is an attempt to explain the observed spatial pattern of the demersal deep-water rose shrimp (*P. longirostris*; 3alpha FAO code: DPS) in the light of the circulation patterns, the presence of strong and persistent surface thermal and chlorophyll fronts and high surface primary production variability in the Strait of Sicily (SoS). We can summarize the results as follows.

1. The spatial distribution of DPS derived from data collected during 2004–2008 bottom trawl surveys in the SoS show maximum concentrations over the eastern slope of the Adventure Bank and along

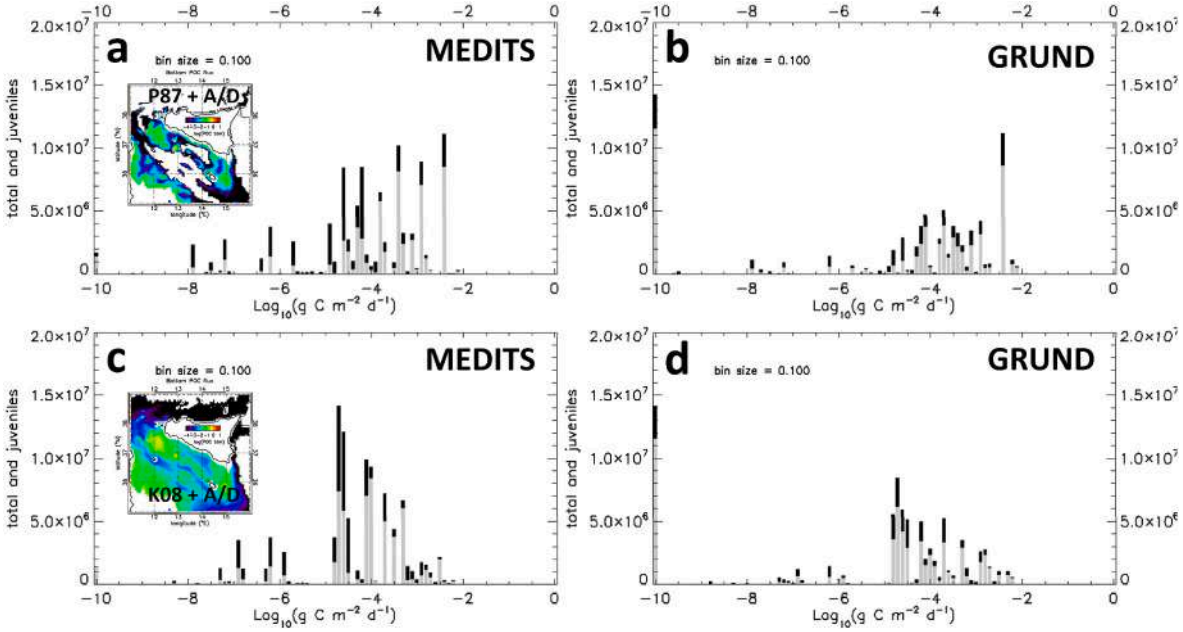

Fig. 10. (a) MEDITS (summer, left panels) and (b) GRUND (fall, right panels) 2004–2008 cumulative abundances vs. POC_{btm}, obtained via the P87 algorithm and advection/diffusion with model horizontal currents (average 2008–2010) and $K_H = 10^7$ cm^2 s^{-1}; (c) and (d) the same, but for POC_{btm} obtained with the K08 algorithm and model currents. Total abundance (in indiv./100 km^2) is expressed by the total height of each histogram bar (grey plus black bar), while grey bars indicate juvenile abundance. Insets reproduce POC_{btm} the spatial distributions of these simulations, i.e. Fig. 8d and 9a.

the southern Sicilian coast. Nonzero DPS abundances are always confined to the upwelling zone (UC) inshore of the AIS, even though with some offshore transport of individuals by means of the upwelling filaments. This spatial distribution is in line with previous studies carried out in different time periods (Fortibuoni et al., 2010; Garofalo et al., 2011; Colloca et al., 2015). This suggests that this distributional pattern is stable over time despite quantitative variations in the more recent years (Sbrana et al., 2019).

2. GAMM analysis shows that DPS juvenile abundance is significantly linked to depth as well as to distance from SST fronts and to front density (i.e. robustness) of chlorophyll fronts.
3. We find that high DPS abundance does not simply superpose spatially to bottom POC fluxes (POC_{btm}) except for a partial overlap in DPS nursery areas, east of Adventure Bank, when these fluxes are computed using 1-D simulations only.
4. However, POC_{btm} fields obtained with simulations using the 1-D model coupled to the horizontal advection/diffusion with model currents in some cases do yield encouragingly high values corresponding to high DPS abundance and nursery sites. This suggests a significant role of ocean circulation and biogeochemical dynamics on DPS abundance, and that DPS juveniles may be trophically closer to benthic POC consumers located where POC_{btm} is more abundant.
5. The simulated POC_{btm} spatial distribution does not change qualitatively when using different horizontal current fields or euphotic zone POC_{50} fields, such as daily/weekly snapshots or single- or multi-year averages. Nevertheless, all simulations to obtain POC_{btm} are highly sensitive to the choice of the 1-D model type for POC sinking and remineralization and the horizontal diffusion coefficient K_H. This represents a caveat for accurate modeling of POC deposition and calls for thorough further investigation.

Future experimental and modeling work should be dedicated to: (1) refining the modeling effort with observation-constrained model parameters; (2) assess whether this methodology may yield the same findings for datasets relative to more recent periods, in which the DPS abundance has varied; (3) investigate the role of water column and near-bottom environmental parameters (dissolved oxygen, water turbidity, etc.) in shaping DPS distribution; (4) fill the gap between the POC flux and the DPS abundance, via further investigation of the diet of its various life stages in the SoS; (5) assessing the temporal variability of what we found in this study, which preliminarily treats the phenomenological situation as stationary.

Improving our understanding of environmental controls on DPS abundance in the Strait of Sicily will allow us to increase predictive capabilities in support of fishery management of this main target species. This not only in that specific area but also in other regions worldwide characterized by high surface primary production and strong vertical motion associated with fronts and upwelling.

Suggested referees

Prof. Andrea Doglioli, MIO - Mediterranean Institute of Oceanography, Campus de Luminy, 13288 Marseille, France. email: andrea.doglioli@univ-amu.fr.

Prof. Marco Zavatarelli, Dipartimento di Fisica e Astronomia - Università di Bologna.

Viale Berti-Pichat 6/2 40127 Bologna, Italia. email: marco.zavatarelli@unibo.it.

Prof. Montserrat Demestre, Instituto de Ciencias del Mer ICM-CSIC, Passeig Marítim de la Barceloneta, 37–49, 08003 Barcelona, Spain. email: montse@icm.csic.es.

Prof. Melissa M. Omand, University of Rhode Island, Graduate School of Oceanography, Narragansett, RI, 02882, USA. email: momand@uri.edu.

Prof. Konstantinos I. Stergiou, Institute of Marine Biological Resources and Inland Waters, Hellenic Centre for Marine Research, 46,7 km Athens Sounio ave., P.O. Box 712, P.C. 19013 Anavyssos, Attiki, Greece. email: kstergio@bio.auth.gr.

Role of the funding source

This work has been supported by: (1) the Italian SSD Pesca project (2011-2015, Italian Ministry of Economics), dedicated to the development of a support and decision system for the sustainability of Southern

Italian fisheries; (2) Parthenope University (Naples, Italy) individual research funds; (3) Project "BASSET-MED: Biodiversity Assessment, Socio-Economic Services, and Evaluation of Anthropogenic Threats in the Central Mediterranean.", part of the Research Projects@CNR 2020.

CRediT authorship contribution statement

Francesco Bignami: Writing – original draft, Supervision, Software, Project administration, Methodology, Investigation, Formal analysis, Conceptualization. **Fabio Fiorentino:** Writing – original draft, Software, Methodology, Investigation, Formal analysis, Data curation, Conceptualization. **Germana Garofalo:** Writing – original draft, Software, Methodology, Investigation, Formal analysis, Data curation, Conceptualization. **Enrico Zambianchi:** Writing – original draft, Methodology, Investigation, Formal analysis, Data curation. **Simone Colella:** Writing – original draft, Methodology, Investigation, Formal analysis, Data curation. **Roberto Sorgente:** Writing – original draft, Methodology, Investigation, Formal analysis, Data curation. **Antonio Olita:** Writing – original draft, Methodology, Investigation, Formal analysis, Data curation. **Angela Landolfi:** Writing – original draft, Methodology, Investigation, Formal analysis, Data curation. **Federico Quattrocchi:** Writing – original draft, Methodology, Investigation, Formal analysis, Data curation. **Peter I. Miller:** Investigation, Conceptualization.

Declaration of competing interest

The authors declare that they have no known competing financial interests or personal relationships that could have appeared to influence the work reported in this paper.

Acknowledgments

We thank: (1) Dr. Bo Zhang (National Institute of Aerospace, USA) for sharing his expertise and providing the code for the Crank-Nicolson diffusion algorithm, which contributed to the success of this research project; (2) Dr. Christophe Brunet of the Stazione Zoologica di Napoli "Anton Dohrn" (Naples, Italy) for fruitful discussion on phytoplankton size range in the Strait of Sicily. This work has been supported by: (1) the Italian SSD Pesca project (2011-2015, Italian Ministry of Economics), dedicated to the development of a support and decision system for the sustainability of Southern Italian fisheries; (2) Parthenope University (Naples, Italy) individual research funds; (3) Project "BASSET-MED: Biodiversity Assessment, Socio-Economic Services, and Evaluation of Anthropogenic Threats in the Central Mediterranean.", part of the Research Projects@CNR 2020.

References

Abella, A., Fiorentino, F., Mannini, A., Orsi Relini, L., 2008. Exploring relationships between recruitment of European hake (*Merluccius merluccius* L. 1758) and environmental factors in the ligurian Sea and the Strait of sicily (central mediterranean). J. Mar. Syst. 71 (3–4), 279–293.

Agnetta, D., Badalamenti, F., Colloca, F., D'Anna, G., Di Lorenzo, M., Fiorentino, F., Garofalo, G., Gristina, G., Labanchi, L., Patti, B., Pipitone, C., Solidoro, C., Libralato, S., 2019. Benthic-pelagic coupling mediates interactions in Mediterranean mixed fisheries: an ecosystem modeling approach. PLoS One 14 (1), e0210659. https://doi.org/10.1371/journal.pone.0210659.

Agostini, V., Bakun, A., 2002. 'Ocean triads' in the Mediterranean Sea: physical mechanisms potentially structuring reproductive habitat suitability (with example application to European anchovy, Engraulis encrasicolus). Fish. Oceanogr. 11, 129–142. https://doi.org/10.1046/j.1365-2419.2002.00201.x.

Alemany, D., Acha, E.M., Iribarne, O.O., 2014. Marine fronts are important fishing areas for demersal species at the Argentine Sea (Southwest Atlantic Ocean). J. Sea Res. 87, 56–67.

Alemany, D., Iribarne, O.O., Acha, E.M., 2018. Marine fronts as preferred habitats for young Patagonian hoki Macruronus magellanicus on the southern Patagonian shelf. Mar. Ecol. Prog. Ser. 588, 191–200.

Ardizzone, G.D., Gravina, M.F., Belluscio, A., Schintu, P., 1990. Depth-size distribution pattern of parapenaeus longirostris (Lucas, 1846) (Decapoda) in the central Mediterranean Sea. J. Crustac Biol. 10 (1), 139–147.

Askari, F., 1998. Remote sensing of topographically-induced upwelling in the southern coastal region of Sicily. SACLANTCEN scientific report n. SR-282-UU, 24 pp. https://apps.dtic.mil/sti/pdfs/AD1113342.pdf.

Askari, F., 2001. Multi-sensor remote sensing of eddy-induced upwelling in the southern coastal region of Sicily. Int. J. Rem. Sens. 22 (15), 2899–2910.

Astraldi, M., Gasparini, G.P., Gervasio, L., Salusti, E., 2001. Dense water dynamics along the Strait of sicily (Mediterranean Sea). J. Phys. Oceanogr. 31 (12), 3457–3475.

Bakun, A., 1998. 'Ocean triads' and radical interdecadal stock variability: bane and boon for fishery management science. In: Pitcher, T.J., Hart, P.J.B., Pauly, D. (Eds.), Reinventing Fisheries Management. Chapman and Hall, London, pp. 331–358.

Bakun, A., Agostini, V.N., 2001. Seasonal patterns of wind-induced upwelling/downwelling in the Mediterranean Sea. Sci. Mar. 65 (3), 243–257.

Basilone, G., Bonanno, A., Patti, B., Mazzola, S., Barra, M., Cuttitta, A., McBride, R., 2013. Spawning site selection by European anchovy (Engraulis encrasicolus) in relation to oceanographic conditions in the strait of Sicily. Fish. Oceanogr. 15 (4), 271–280.

Baustian, M.M., Hansen, G.J.a., de Kluijver, A., Robinson, K., Henry, E.N., Knoll, L.B., et al., 2014. Linking the bottom to the top in aquatic ecosystems: mechanisms and stressors of benthic-pelagic coupling. Eco-DAS X Symp Proc. 25–47.

Béranger, K., Mortier, L., Gasparini, G., Gervasio, L., Astraldi, M., Crépon, M., 2004. The dynamic of the Sicily Strait: a comprehensive study from observations and models. Deep-Sea Res. Part II 51 (4–5), 411–440.

Bertrand, J.A., Gil de Sola, L., Papaconstantinou, C., Relini, G., Souplet, A., 2002. The general specifications of the MEDITS surveys. Sci. Mar. 66 (2), 9–17.

Biggs, D.C., Hu, C., Muller-Karger, F.E., 2008. Remotely sensed sea-surface chlorophyll and POC flux at deep Gulf of Mexico benthos sampling stations. Deep-Sea Res. Part II 55, 2555–2562. https://doi.org/10.1016/j.dsr2.2008.07.013.

Bignami, F., Böhm, E., D'Acunzo, E., D'Archino, R., Salusti, E., 2008. On the dynamics of surface cold filaments in the Mediterranean Sea. J. Mar. Syst. 74, 429–442.

Buongiorno Nardelli, B., Santoleri, R., Iudicone, D., Zoffoli, S., 1999. Altimetric signal and three-dimensional structure of the sea in the Channel of Sicily. J. Geophys. Res. 104 (C9), 20,585-20,603.

Carlucci, R., Gancitano, V., 2015. Parapenaeus longirostris. In: Sartor, P., Mannini, A., Carlucci, R., Massaro, E., Queirolo, S., Sabatini, A., Scarcella, G., Simoni, R. (Eds.), Sintesi delle conoscenze di biologia, ecologia e pesca delle specie ittiche dei mari italiani. Biol. Mar. Mediterr., p. 22. Suppl.

Cartes, J.E., López-Pérez, C., Carbonell, A., 2018. Condition and recruitment of Aristeus antennatus at great depths (to 2,300 m) in the Mediterranean: relationship with environmental factors. Fish. Oceanogr. 27 (2), 114–126. https://doi.org/10.1111/fog.12237.

Cianelli, D., Sarno, D., D'Alelio, D., Zingone, A., Zambianchi, E., Uttieri, M., d'Alcalà, M. R., 2017. Disentangling physical and biological drivers of phytoplankton dynamics in a coastal system. Sci. Rep. 7 (1), 15868 https://doi.org/10.1038/s41598-017-15880-x.

Colella, S., 2006. La produzione primaria nel Mar Mediterraneo da satellite: sviluppo di un modello regionale e sua applicazione ai dati SeaWiFS, MODIS e MERIS. Dottorato Scienze ed Ingegneria del Mare XIX ciclo, Università degli Studi di Napoli "Parthenope". PhD Dissertation. http://www.fedoa.unina.it/1660/1/Colella_Scienze_Ingegneria.pdf.

Colloca, F., Garofalo, G., Bitetto, I., Facchini, M.T., Grati, F., Martiradonna, A., Mastrantonio, G., Nikolioudakis, N., Ordinas, F., Scarcella, G., Tserpes, G., Pilar Tugores, M., Valavanis, V., Carlucci, R., Fiorentino, F., Follesa, M.C., Iglesias, M., Knittweis, L., Lefkaditou, E., Lembo, G., Manfredi, C., Massutí, E., Pace, M.L., Papadopoulou, N., Sartor, P., Smith, C.J., Spedicato, M.T., 2015. The seascape of demersal fish nursery areas in the north Mediterranean Sea, a first step towards the implementation of spatial planning for trawl fisheries. PLoS One 10 (3), e0119590. https://doi.org/10.1371/journal.pone.0119590.

Corrado, R., Lacorata, G., Palatella, L., Santoleri, R., Zambianchi, E., 2017. General characteristics of relative dispersion in the ocean. Sci. Rep. 7, 46291. https://doi.org/10.1038/srep46291.

Demarcq, H., Faure, V., 2000. Coastal upwelling and associated retention indices derived from satellite SST. Application to Octopus vulgaris recruitment. Oceanol. Acta 23 (4), 391–408.

D'Ortenzio, F., Iudicone, D., Montegut, C.D., Testor, P., Antoine, D., Marullo, S., Santoleri, R., Madec, G., 2005. Seasonal variability of the mixed layer depth in the Mediterranean Sea as derived from in situ profiles. Geophys. Res. Lett. 32, L12605 https://doi.org/10.1029/2005GL022463.

Druon, J.-N., Fromentin, J.-M., Aulanier, F., Heikkonen, J., 2011. Potential feeding and spawning habitats of Atlantic bluefin tuna in the Mediterranean Sea. Mar. Ecol. Prog. Ser. 439, 223–240.

Druon, J.-N., Fiorentino, F., Murenu, M., Knittweis, L., Colloca, F., Osio, C., Mérigot, B., Garofalo, G., Mannini, A., Jadaud, A., Sbrana, M., Scarcella, G., Tserpes, G., Peristeraki, P., Carlucci, R., Heikkonen, J., 2015. Modelling of European hake nurseries in the Mediterranean Sea: an ecological niche approach. Prog. Oceanogr. 130, 188–204. https://doi.org/10.1016/j.pocean.2014.11.005.

Druon, J.-N., Gascuel, D., Gibin, M., Zanzi, A., Fromentin, J., Colloca, F., Hélaouët, P., Coll, M., Mannini, A., Bluemel, J.K., Piroddi, C., Bastardie, F., Macias-Moy, D., Vasilakopoulos, P., Winker, H., Serpetti, N., Guillen, J., Palialexis, A., Gras, M., Hekim, Z., Dubroca, L., Pinto, C., Steenbeek, J., Martinsohn, J., 2021. Mesoscale productivity fronts and local fishing opportunities in the European Seas. Fish Fish. 22, 1227–1247.

Emerson, S., Hedges, J.I., 1988. Processes controlling the organic carbon content of open ocean sediments. Paleoceanography 3, 621–634.

Falcini, F., Palatella, L., Cuttitta, A., Buongiorno Nardelli, B., Lacorata, G., Lanotte, A.S., Patti, B., Santoleri, R., 2015. The role of hydrodynamic processes on anchovy eggs and larvae distribution in the Sicily Channel (Mediterranean Sea): a case study for

the 2004 data set. PLoS One 10 (4), e0123213. https://doi.org/10.1371/journal.pone.0123213.
FAO GFCM, 2009. Establishment of Geographical Sub-Areas in the GFCM area amending the resolution GFCM/31/2007/2. RES-GFCM/33/2009/2, 5pp. http://www.fao.org/3/a-ax817e.pdf.
Fortibuoni, T., Bahri, T., Camilleri, M., Garofalo, G., Gristina, M., Fiorentino, F., 2010. Nursery and spawning areas of deep-water rose shrimp, Parapenaeus longirostris (Decapoda: penaeidae), in the Strait of Sicily. J. Crustac Biol. 30, 167–174.
Garcìa Lafuente, J., 2002. Hydrographic phenomena influencing early life stages of the Sicilian Channel anchovy. Fish. Oceanogr. 11 (1), 31–44.
Gargano, F., Garofalo, G., Fiorentino, F., 2017. Exploring connectivity between spawning and nursery areas of Mullus barbatus (L., 1758) in the Mediterranean through a dispersal model. Fish. Oceanogr. 26 (4), 476–497. https://doi.org/10.1111/fog.12210.
Gargano, F., Garofalo, G., Quattrocchi, F., Fiorentino, F., 2022. Where do recruits come from? Backward Lagrangian simulation for the deep water rose shrimps in the Central Mediterranean Sea. Fish. Oceanogr. 31 (4), 369–383. https://doi.org/10.1111/fog.12582.
Garofalo, G., Fortibuoni, T., Gristina, M., Sinopoli, M., Fiorentino, F., 2011. Persistence and co-occurrence of demersal nurseries in the Strait of Sicily (Central Mediterranean): implications for fishery management. J. Sea Res. 66, 29–38.
Giannoulaki, M., Belluscio, A., Colloca, F., Fraschetti, S., Scardi, M., Smith, C., Panayotidis, P., Valavanis, V., Spedicato, M.T., 2013. Mediterranean sensitive habitats. DG MARE Specific Contract SI2.600741 557. Final Report. http://imbriw.hcmr.gr/en/wp-content/uploads/2013/12/MEDISEH-final-report-reduced.pdf.
Griffiths, J.R., Kadin, M., Nascimento, F.J.A., Tamelander, T., Törnroos, A., Bonaglia, S., et al., 2017. The importance of benthic-pelagic coupling for marine ecosystem functioning in a changing world. Global Change Biol. 23, 2179–2196. https://doi.org/10.1111/gcb.13642.
Hastie, T.J., Tibshirani, R.J., 1990. Generalised Additive Models. St. Edmundsbury Press Limited, Suffolk, UK.
Heldt, J.H., 1938. La production chez les crustacés décapodes de la famile des pénéidés. Ann. Inst. Océanogr. Monaco 18, 31–206.
Houghton, R.W., Marra, J., 1983. Physical/biological structure and exchange across the thermohaline shelf/slope front in the New York Bight. J. Geophys. Res. 88 (C7), 4467–4481.
Kapiris, K., 2004. Feeding ecology of parapenaeus longirostris (Lucas, 1846) (Decapoda: penaeidae) from the Ionian Sea (central and eastern Mediterranean Sea). Sci. Mar. 68 (2), 247–256.
Klein, P., Lapeyre, G., 2009. The oceanic vertical pump induced by mesoscale and submesoscale turbulence. Ann. Rev. Mar. Sci 1, 351–375.
Knittweis, L., Arneri, E., Ben Meriem, S., Dimech, M., Fiorentino, F., Gancitano, V., Jarboui, O., Mbarek, K.B., Ceriola, L., 2013. Stock status and potential yield of deep water rose shrimp (Parapenaeus longirostris, Lucas 1846) in the south-central Mediterranean Sea. MedSudMed Technical Documents. No. 28. GCP/RER/010/ITA/MSM-TD-28 15.
Kriest, I., Oschlies, A., 2008. On the treatment of particulate organic matter sinking in large-scale models of marine biogeochemical cycles. Biogeosciences 5, 55–72.
Lermusiaux, P.F.J., Robinson, A.R., 2001. Features of dominant mesoscale variability, circulation patterns and dynamics in the Strait of Sicily. Deep Sea Res. 48 (Part I), 1953–1997.
Levi, D., Andreoli, M.G., Giusto, R.M., 1995. First assessment of the rose shrimp, *parapenaeus longirostris* (Lucas 1846), in the central mediterranean. Fish. Res. 21, 375–393.
Lévy, M., Ferrari, R., Franks, P., Martin, A., Riviere, P., 2012. Bringing physics to life at the submesoscale. Geophys. Res. Lett. 39, L14602.
Lucas, H., 1846. Crustacés, arachnides, myriapodes, et hexapodes. Exploration Scientifique de l'Algérie pendant les années 1840, 1841–1842. Sciences physiques. Zoologie I. Histoire Naturelle des Animaux Articulés. (Paris) 1, 1-403, pls. 1-8, available at: http://biodiversitylibrary.org/page/46116712.
Lumpkin, R., Pazos, M., 2007. Measuring surface currents with Surface Velocity Program drifters: the instrument, its data, and some recent results. In: Griffa, A., Kirwan, Jr.A. D., Mariano, A.J., Özgökmen, T., Rossby, H.T. (Eds.), Lagrangian Analysis and Prediction of Coastal and Ocean Dynamics. Cambridge University Press, pp. 39–67.
Marin, J., 2009. Shrimps and krill. In: Safran, P. (Ed.), Fisheries and Aquaculture V. II. EOLSS Publishers, Oxford, UK.
Martin, J., Knauer, G., Karl, D., Broenkow, W., 1987. VERTEX: carbon cycling in the Northeast Pacific. Deep-Sea Res. 34, 267–285.
Miller, P.I., 2009. Composite front maps for improved visibility of dynamic sea-surface features on cloudy SeaWiFS and AVHRR data. J. Mar. Syst. 78 (3), 327–336. https://doi.org/10.1016/j.jmarsys.2008.11.019.
Miller, P.I., Scales, K.L., Ingram, S.N., Southall, E.J., Sims, D.W., 2015. Basking sharks and oceanographic fronts: quantifying associations in the north-east Atlantic. Funct. Ecol. 29 (8), 1099–1109. https://doi.org/10.1111/1365-2435.12423.
Mori, M., Sartor, P., Biagi, F., 2000. Diet of adult females of Parapenaeus longirostris (Crustacea, Decapoda) in the northern Tyrrhenian Sea (western Mediterranean). Atti Soc. Toscana. Sci. Nat. Mem. 107 (B), 7–10.
Morse, J.W., Beazley, M.J., 2008. Organic matter in deepwater sediments of the Northern Gulf of Mexico and its relationship to the distribution of benthic organisms. Deep Sea Res. Part II 55, 2563–2571.
Muller-Karger, F.E., Varela, R., Thunell, R., Luerssen, R., Hu, C., Walsh, J.J., 2005. The importance of continental margins in the global carbon cycle. Geophys. Res. Lett. 32, L01602 https://doi.org/10.1029/2004GL021346.
Munk, P., Larsson, P.O., Danielssen, D.S., Moksness, E., 1999. Variability infrontal zone formation anddistribution of gadoid fish larvae at the shelf break in the northeastern North Sea. Mar. Ecol. Prog. Ser. 177, 221–233.
Nouar, A., Kennouche, H., Ainoucheand, N., Cartes, J.E., 2011. Temporal changes in the diet of deep-water Penaeoidean shrimp (*Parapenaeus longirostris* and *Aristeus antennatus*) off Algeria (southwestern Mediterranean). Sci. Mar. 75 (2), 279–288.
Olita, A., Dobricic, S., Ribotti, A., Fazioli, L., Cucco, A., Dufau, C., Sorgente, R., 2012. Impact of SLA assimilation in the Sicily Channel regional model: model skills and mesoscale features. Ocean Sci. 8 (4), 485–496.
Pace, M.L., Kanuer, G.A., Karl, D.M., Martin, J.H., 1987. Primary production, new production, and vertical flux in the eastern Pacific Ocean. Nature 325, 803–804.
Patti, B., Torri, M., Cuttitta, A., 2020. General surface circulation controls the interannual fluctuations of anchovy stock biomass in the Central Mediterranean Sea. Sci. Rep. 10 (1), 1554.
Piccioni, A., Gabriele, M., Salusti, E., Zambianchi, E., 1988. Wind-induced upwellings off the southern coast of Sicily. Oceanol. Acta 11 (4), 309–314.
Pisano, A., De Dominicis, M., Biamino, W., Bignami, F., Gherardi, S., Colao, F., Coppini, G., Marullo, S., Sprovieri, M., Trivero, P., Zambianchi, E., Santoleri, R., 2016. An oceanographic survey for oil spill monitoring and model forecasting validation using remote sensing and in situ data in the Mediterranean Sea. Deep Sea Res. Part II 133, 132–145. https://doi.org/10.1016/j.dsr2.2016.02.013.
Politou, C.-Y., Tserpes, G., Dokos, J., 2008. Identification of deep-water pink shrimp abundance distribution patterns and nursery grounds in the eastern Mediterranean by means of generalized additive modeling. Hydrobiologia 612, 99–107.
Polunin, N.V.C., Morales-Nin, B., Pawsey, W.E., Cartes, J.E., Pinnegar, J.K., Moranta, J., 2001. Feeding relationships in Mediterranean bathyal assemblages elucidated by stable nitrogen and carbon isotope data. Mar. Ecol. Prog. Ser. 220, 13–23. https://doi.org/10.3354/meps220013.
Poulain, P.-M., Zambianchi, E., 2007. Surface circulation in the central Mediterranean Sea as deduced from Lagrangian drifters in the 1990s. Continent. Shelf Res. 27, 981–1001.
Poulain, P.-M., Menna, M., Mauri, E., 2012. Surface geostrophic circulation of the Mediterranean Sea derived from drifter and satellite altimeter data. J. Phys. Oceanogr. 42 (6), 973–990.
Quattrocchi, G., Sinerchia, M., Colloca, F., Fiorentino, F., Garofalo, G., Cucco, A., 2019. Hydrodynamic controls on connectivity of the high commercial value shrimp Parapenaeus longirostris (Lucas, 1846) in the Mediterranean Sea. Sci. Rep. 9, 16935 https://doi.org/10.1038/s41598-019-53245-8.
R Development Core Team, 2011. R: A Language and Environment for Statistical Computing. R Foundation for Statistical Computing, Vienna, Austria. http://www.R-project.org/.
Relini, G., 2000. Demersal trawl surveys in Italian seas: a short review. In: Bertrand, J.A., Relini, G. (Eds.), Demersal Resources in the Mediterranean. Proceedings of the symposium held in Pisa, 18–21 March 1998. Actes de Colloques, vol. 26. IFREMER, Plouzané, pp. 76–93.
Rinaldi, E., Buongiorno Nardelli, B., Volpe, G., Santoleri, R., 2014. Chlorophyll distribution and variability in the Sicily Channel (Mediterranean Sea) as seen by remote sensing data. Continent. Shelf Res. 77, 61–68. https://doi.org/10.1016/j.csr.2014.01.010.
Robinson, A.R., Sellschopp, J., Warn-Varnas, A., Leslie, W.G., Lozano, C.J., Haley Jr., P. J., Anderson, L.A., Lermusiaux, P.F.J., 1999. The atlantic ionian Stream. J. Mar. Syst. 20, 129–156.
Rodríguez-Climent, S., Sonderblohm, C.P., Fonseca, P., Erzini, K., Campos, A., 2016. Diel variation in the deep-water rose shrimp Parapenaeus longirostris (Lucas, 1846) catches off the Portuguese south coast. Front. Mar. Sci. Conference Abstract: XIX Iberian Symposium on Marine Biology Studies. https://doi.org/10.3389/conf.FMARS.2016.05.00073.
Rowe, G.T., Mahlon, C.K., 2008. Introduction to the deep Gulf of Mexico benthos program. Deep-Sea Res. Part II 55, 2536–2540.
Sbrana, M., Zupa, W., Ligas, A., Capezzuto, F., Chatzispyrou, A., Follesa, M.C., Gancitano, V., Guijarro, B., Isajlovic, I., Jadaud, A., Markovic, O., Micallef, R., Peristeraki, P., Piccinetti, C., Thasitis, I., Carbonara, P., 2019. Spatiotemporal abundance pattern of deep-water rose shrimp, Parapenaeus longirostris, and Norway lobster, Nephrops norvegicus. In: European Mediterranean waters. Sci. Mar. 83 (S1), 71–80. https://scientiamarina.revistas.csic.es/index.php/scientiamarina/article/view/1797.
Scales, K.L., Miller, P.I., Hawkes, L.A., Ingram, S.N., Sims, D.W., Votier, S.C., 2014. On the Front Line: frontal zones as priority at-sea conservation areas for mobile marine vertebrates. J. Appl. Ecol. 51 (6), 1575–1583. https://doi.org/10.1111/1365-2664.12330.
Scalisi, M., Levi, D., Fiorentini, L., Giusto, G.B., Palumbo, V., Rizzo, P., 1998. Experimental approach to intercalibrate data of trawl surveys conducted with different nets. Biol. Mar. Mediterr. 5, 40–51.
Siegel, D.A., Deuser, W.G., 1997. Trajectories of sinking particles in the Sargasso Sea: modeling of statistical funnels above deep-ocean sediment traps. Deep-Sea Res., Part A I 44 (9–10), 1519–1541.
Sobrino, I., Silva, C., Sbrana, M., Kapiris, K., 2005. A review of the biology and fisheries of the deep water rose shrimp, Parapenaeus longirostris, in European Atlantic and Mediterranean waters (decapoda, dendrobranchiata, penaeidae). Crustaceana 78 (10), 1153–1184.
Sorgente, R., Olita, A., Oddo, P., Fazioli, L., Ribotti, A., 2011. Numerical simulation and decomposition of kinetic energy in the Central Mediterranean: insight on mesoscale circulation and energy conversion. Ocean Sci. 7, 503–519. https://doi.org/10.5194/os-7-503-2011.
Tecchio, S., Coll, M., Sardà, F., 2015. Structure, functioning, and cumulative stressors of Mediterranean deepsea ecosystems. Prog. Oceanogr. 135, 156–167. https://doi.org/10.1016/j.pocean.2015.05.018.
Volpe, G., Santoleri, R., Vellucci, V., Ribera d'Alcalà, M., Marullo, S., D'Ortenzio, F., 2007. The colour of the Mediterranean Sea: global versus regional bio-optical

algorithms evaluation and implication for satellite chlorophyll estimates. Rem. Sens. Environ. 107, 625–638.
Wood, S.N., 2006. Generalized Additive Models: an Introduction with R. Chapman & Hall, London.
Zambianchi, E., Trani, M., Falco, P., 2017. Lagrangian transport of marine litter in the Mediterranean Sea. Front. Environ. Sci. 5, 1–15. https://doi.org/10.3389/fenvs.2017.00005.
Zervoudaki, S., Nielsen, T.G., Christou, E.D., Siokou-Frangou, I., 2006. Zooplankton distribution and diversity in a frontal area of the Aegean Sea. Mar. Biol. Res. 2 (3), 149–168. https://doi.org/10.1080/17451000600702037.
Zuur, A.F., Ieno, E.N., Smith, G.M., 2007. Analysing Ecological Data. Springer, New York.
Zuur, A.F., Ieno, E.N., Walker, N.J., Saveliev, A.A., Smith, G., 2009. Mixed Effects Models and Extensions in Ecology. Springer, New York.